Ruthenium Carbon-Rich Group as a Redox-Switchable Metal Coupling Unit in Linear Trinuclear Complexes

E. Di Piazza, C. Boilleau, A. Vacher, K. Merahi, L. Norel, K. Costuas, T. Roisnel, S. Choua, P. Turek, S. Rigaut

Ruthenium Carbon-Rich Group as Redox Switchable Metal Coupling Unit in Linear Trinuclear Complexes

Emmanuel Di Piazza,[†] Corentin Boilleau,[†,#] Antoine Vacher,[†] Khalissa Merahi,[‡] Lucie Norel,[†] Karine Costuas,[†] Thierry Roisnel,[†] Sylvie Choua,[‡]* Philippe Turek,[‡] and Stéphane Rigaut[†]**

† UMR 6226 CNRS - Université de Rennes 1, Institut des Sciences Chimiques de Rennes, Campus de Beaulieu, F-35042, Rennes Cedex, France

‡ UMR 7177 CNRS - Université de Strasbourg, Institut de Chimie, 1 rue Blaise Pascal, BP 296 R8, F-67008 Strasbourg Cedex, France

* To whom correspondence should be addressed. E-mail: sylvie.choua@unistra.fr, karine.costuas@univ-renes1.fr, stephane.rigaut@univ-rennes1.fr

[#] Present address: Institute of Physics, Polish Academy of Sciences, Warsaw, Poland

RECEIVED DATE (to be automatically inserted after your manuscript is accepted if required according to the journal that you are submitting your paper to)

TITLE RUNNING HEAD: Ruthenium Carbon-Rich Group as Redox Switchable Metal Coupling Units in Linear Trinuclear Complexes

[†] UMR 6226 CNRS - Université de Rennes 1

‡ UMR 7177 CNRS - Université de Strasbourg

Abstract. The preparation and the properties of novel ruthenium carbon-rich complexes [(Ph-C≡C-)$_{2-n}$Ru(dppe)$_2$(-C≡C-bipyM(hfac)$_2$)$_n$] (n = 1, 2 ; M = Cu^{II}, Mn^{II} , bipy = 2,2'-bipyridine-5-yl) characterized with single-crystal X-ray diffraction and deigned for molecular magnetism are reported. With the help of EPR spectroscopy, we show that the neutral ruthenium system sets up a magnetic coupling between two remote paramagnetic Cu^{II} units. More specifically, these copper compounds are unique examples of bimetallic and linear heterotrimetallic compounds for which a complete rationalization of the magnetic interactions could be made for exceptionally long distances between the spin carriers (8.3 Å between adjacent Cu and Ru centers, 16.6 Å between external Cu centers) and compared at two different redox states. Surprisingly, oxidation of the ruthenium redox-active metal coupling unit (MCU), that introduces an additional spin unit on the carbon-rich part, leads to weaker magnetic interactions. On the contrary, in the simpler parent complexes bearing only one paramagnetic metal unit [Ph-C≡C-Ru(dppe)$_2$-C≡C-bipyCu(hfac)$_2$], one electron oxidation of the ruthenium diethynyl unit generates an interaction between the Cu and Ru spin carriers of comparable magnitude to that observed between the two far apart Cu ions in the above corresponding neutral trimetallic system. Evaluation and rationalization of those coupling with theoretical tools are in rational agreement with experiments for such complex systems.

Keywords: Magnetism, Redox switch, Ruthenium, Metal coupling unit, Carbon-rich system, EPR spectroscopy. Theoretical calculations

Introduction

A great challenge to contemporary applied science is to develop molecular-based switching devices in which one or several key physical properties can be modulated with external stimuli, such as light or electricity,[1-3] for the realization of logical functions.[1, 4] In that direction, colour, luminescence, optical nonlinearity, magnetic and electrochemical properties, as well as changes in electrical conductivity are frequently used for memory or sensing applications, and multifunctional molecules are susceptible to perform new properties or operations unattainable by conventional semi-conductor technology.

For this purpose, transitionmetal acetylide are attractive redox active building blocks.[5-11] They present fast and discrete interfacial electron transfers,[12-16] and allowed modulation of different features such as NLO,[17-19] luminescent,[20-22] or other optical properties,[10, 23-27] as well as magnetism[23, 28-31]and conductivity.[32-46] Among all studied systems, ruthenium acetylides with a *trans* ditopic structure are particularly well suited owing to their unique ability to operate as a connector allowing electron flow to occur through different elements in multi-component systems.[29, 47-51] This behavior results from the substantial carbon-chain ligand character of the highest occupied molecular orbital (HOMO) due to the overlap of a metal d(π) and of a delocalized π-orbital of the carbon-rich ligand.

Interestingly, concerning molecular magnetism, very few reports have been published on the capacity of such organometallic moieties to act as magnetic coupling units (MCU) between remote radicals, despite the fact that this research area is very attractive with respect to the promising new materials that might be prepared.[52-54] While molecular packing occurring in crystal usually leads to weak intermolecular interactions, the use of a MCU allows intramolecular interactions to set up between radical connected through. In parallel, the remote control of magnetism with stimuli such as light or electron transfer is also very appealing.[2, 55] Light-controlled systems are well developed with numerous type of systems, however, redox-controllable systems are much scarcer.[56-71] Hence, as far as metal acetylide are concerned, the first study reported a platinum bis-ethynyl-phenyl-nitronyl-nitroxide complex displaying a weak coupling between the two radicals ($0.1 < |J| < 1$ cm^{-1}, 18.6 Å

separating the two spin carriers) through the non-redox active diamagnetic transition Pt MCU, being known to be an inefficient mediator.[72] More recently, we reported the first use of the redox active fragment [Ru(dppe)$_2$(C≡CR)$_2$] (dppe = 1,2-bis(diphenylphosphino)ethane) (Chart 1) with orbitals delocalized on both metal centre and acetylide ligands, to evaluate (i) their ability to set up a magnetic coupling between one or two remote organic spin carrier(s) and nature of the resulting exchange interaction (ferromagnetic or antiferromagnetic), and (ii) the effect of its one electron oxidation, that creates an additional (de)localized spin, on the magnetic properties. It occurred that the diamagnetic [Ru(dppe)$_2$(-C≡C-R)$_2$] system is able to promote a stronger magnetic coupling between two remote radical units, i.e. nitronyl nitroxide (NN) (-2 cm^{-1}, estimated distance 19.3 Å) or two verdazyl radicals (VD) (-4 cm^{-1}, estimated distance 19.1 Å) than the Pt unit.[73] Unexpectedly, while introducing an additional spin carrier on the metal MCU, oxidation leads to the decrease or the switching off of magnetic interactions, whereas one electron oxidation of the monoradical species [Ph-C≡C-Ru(dppe)$_2$-C≡C-R] generates an antiferromagnetic spin alignment between the two spin carries of ca. 2 cm^{-1} and 4 cm^{-1} for nitronyl-nitroxide and verdazyl radicals, respectively.

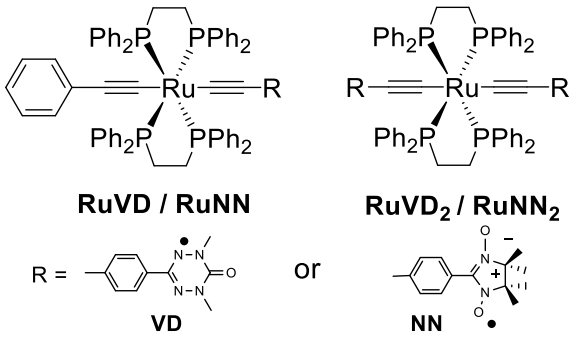

Chart 1

In order to understand the magnetic behavior of such redox active assemblies through the rationalization of the different interactions that can exist in such compounds, we further designed new mono- and bi-nuclear metal acetylide complexes [(Ph-C≡C-)$_{2-n}$Ru(dppe)$_2$(-C≡C-bipyM(hfac)$_2$)$_n$] (n = 1, 2 ; M = Cu^{II}, Mn^{II}, bipy = 2,2'-bipyridine-5-yl) bearing inorganic radicals (scheme 1),[74] (i) to set up a new magnetic coupling, and (ii) to achieve the redox modulation/creation of exchange interactions between the different elements of those assemblies. Note, the ruthenium acetylide system displays a sufficiently low oxidation potential (E° = 0.5 V vs SCE) to avoid oxidations of Cu^{II} and Mn^{II} centers.[75]

Note that this 2,2'-bipyridine-5-yl positioning was chosen because 4-yl positioning would create a spin frustration between Mn/Cu and Ru spin carriers and annihilate a probable polarization mechanism magnetic coupling (Ovchinnikov rule). Therefore, in this article we describe the synthesis and the characterization of these new complexes including the crystallographic structures, the electrochemical and the electronic absorption properties. With Cu complexes, the strength of the intramolecular interactions were addressed in the isolated state (dilute solution) with EPR spectroscopy. The study of the magnetic interactions in the present systems is particularly challenging taking into account the number of parameters that could be introduce in order to fit the experimental curves. Thus, we conducted a parallel quantum chemical DFT study that provides important information on the geometrical, electronic and magnetic changes of the systems occurring upon oxidation of the ruthenium core.

Results and discussion

Syntheses of the heteronuclear complexes. The synthetic strategy to achieve the heteronuclear complexes terminated is displayed on Scheme 1. Coordination of various metals to bipyridine-functionalized ruthenium acetylides has been reported by several groups, including our group.[20, 21, 30, 31, 76-78] Thus, reaction of the previously reported complex[20, 21] **1** and **2** with $[M^{II}(hfac)_2(H_2O)_2]$ (M = Cu, Mn) was achieved by displacement of the labile water molecules by the 2,2'-bipyridyl-ligand.[79] More precisely, combinations of equimolar quantities of $[M^{II}(hfac)_2(H_2O)_2]$ and of bipyridine complex **1** or **2** in toluene under mild conditions lead to the precipitation of the desired complex **1Cu** or **1Mn** and **2Cu** or **2Mn**. In addition to the accurate results from high resolution mass-spectrometry (HRMS), the FTIR measurements shows for the four adducts a consistent shift of the initial $\nu_{(C\equiv C)}$ at 2057 and 2062 cm^{-1} for **1** and **2**, respectively, to lower energies for the heavier substituents at 2030-2040 cm^{-1} (Table 1). The carbonyl vibration stretches for the hfac ligand were observed at ca. 1670 and 1650 cm^{-1} for the Cu and Mn adducts, respectively, consistent with our analogous lanthanide complexes.[21]

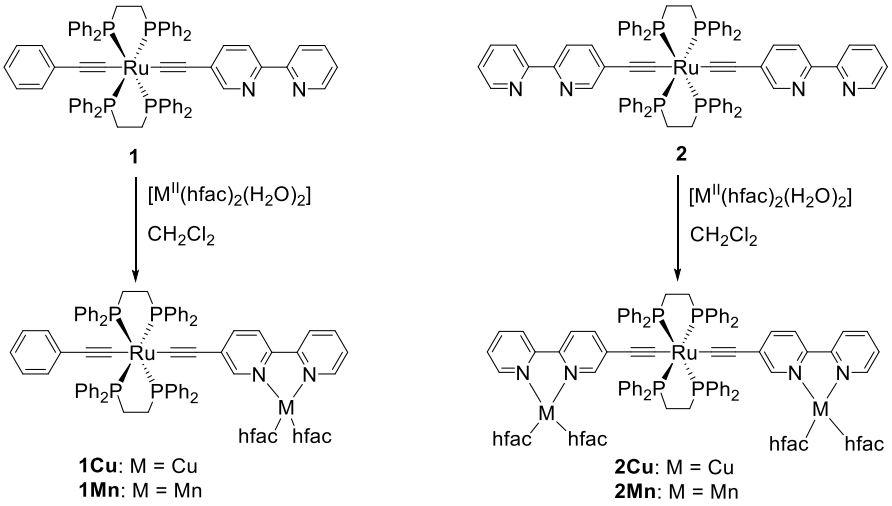

Scheme 1. Synthetic pathways yielding the heterometallic complexes.

Table 1. Infrared (IR), electrochemical (CV) and UV-vis data.

	IR $\nu_{C\equiv C}$ (cm^{-1})		Electrochemistry[a,b] $E°$ (V)			UV-Vis[d] λ_{max}/nm (ε /mol^{-1}.L.cm^{-1})	
	n = 0	n = 1	E°(0/-)	E°(+/0)	E°(2+/+)	n = 0	n = 1
1Cu $^{n+}$	2040	1910	-0.798 [c]	0.118	0.924[c]	308 (35500), 494 (22700)	306(45348), 494(8134), 1044(5219)
1Mn $^{n+}$	2039			0.094	0.912[c]	308 (42400), 468 (19600)	308(50600), 470(6200), 1040(4500)
2Cu $^{n+}$	2036	1938	-0.652 [c]	0.333	-	308 (42400), 494 (44200)	302(45389), 382(42000), 494(21304), 1 059(6391)
2Mn $^{n+}$	2042			0.271	-	306 (34400), 468 (27100)	306(43569), 376(26073), 462(11901), 1060 (2972)

[a] Sample 1 mM, Bu_4NPF_6 (0.1 M) in CH_2Cl_2, v = 100 mV·s^{-1}, potentials are reported in V *vs.* FcH/FcH^+ as an internal standard. [b] Reversible oxidation processes, ΔE_p≈60-70 mV. [c] Peak potential of an irreversible process. [d] In CH_2Cl_2.

Table 2. Crystal data and structure refinements for **1Cu**, **1Mn**, **2Cu**, **2Mn**

	1Cu	**1Mn**	**2Cu**	**2Mn**
Formula	$2(C_{82}H_{62}CuF_{12}N_2O_4P_4Ru)$	$2(C_{82}H_{62}F_{12}MnN_2O_4P_4Ru), CH_2Cl_2$	$C_{96}H_{66}Cu_2F_{24}N_4O_8P_4Ru$	$C_{96}H_{66}F_{24}Mn_2N_4O_8P_4Ru$
FW	3311.65	3379.38	2211.56	2194.36
Cryst. Syst.	monoclinic	monoclinic	triclinic	triclinic
Space group	C c	C c	P -1	P -1
a (Å)	23.5501(8)	23.4303(7)	12.5151(6)	12.6560(5)
b (Å)	25.9572(10)	26.4469(9)	14.2018(7)	12.8898(5)
c (Å)	29.1399(12)	29.1729(8)	16.9346(9)	17.5101(7)
α (°)	90	90	78.404(2)	88.558(2)
β (°)	109.0540(10)	108.1130(10)	82.063(2)	84.096(2)
γ (°)	90	90	78.333(2)	60.718(2)
V ($Å^3$)	16837.1(11)	17181.4(9)	2872.6(2)	2477.23(17)
Z	4	4	1	1
D_{ca} ($g.cm^{-3}$)	1.306	1.306	1.278	1.471
T (K)	100(2)	100(2)	100(2)	100(2)
Final R	0.0613	0.0365	0.0609	0.0372
R_w	0.1547	0.0967	0.1625	0.0953

X-Ray analysis. Good quality crystals suitable for X-Ray structure determination were obtained from a methylene chloride/n-pentane biphasic mixture (2/1) for all compounds. The crystallographic data are listed in Table 2. The labeled plots excluding solvent molecules are reported in Figure 1-6 and bond lengths and angles are given in Table S1. The two bimetallic complexes **1Cu** and **1Mn** are iso-structural and crystallize in the monoclinic (Cc) space group (Figure 1 and 2). The unit cell includes two molecules (Figure 3). The acetylide bonding between the ruthenium atom and the bipyridyl moieties is barely affected by the coordination as previously observed.[21, 30, 77, 80] The two pirydine rings of the 2,2'-bipyridyl moieties binding the metal atom lie in the same plane (the angle between the rings of the bpy ligand mean planes being 3.01 and 8.77° for **1Cu**, and 8.84 and 10.65° for **1Mn**, respectively), and π–π stacking is observed between the bipyridine ligands of two molecules of the unit cell to form pairs that are characterized by interplanar distance in the range of 3.5 – 3.7 Å (Figure 3). Therefore, inter-molecular metal-metal distances for the solid-state arrangements of **1Mn** and **1Cu** are found to be 7.437 Å between the closest Mn atoms and 7.107 Å between the closest Cu ones.

The M1 center (M = Mn, Cu) are coordinated to the oxygen atoms from the two bidentates $hfac^-$ anions and to the two nitrogen atoms N7 and N14 from the bipyridyl units with distorted octahedral coordination geometries. The elongation axis for the copper moiety in **1Cu** is through the O101-Cu1-O104 axis (Figure 1 and Table S1). Therefore, these two oxygen atoms from the hfac ligands are ligated in the axial positions and the residual two hfac oxygen atoms are ligated in the equatorial positions along with the bipyridyl units with a bite angle of 81.75(19)°. The angles between the axial and equatorial ligands slightly deviate from 90°. The geometry of the second molecule is essentially the same with a Cu2 center showing a Jahn-Teller elongation along an O-Cu-O axis. Concerning **1Mn**, the Mn1 ion is six coordinated but its geometry deviates more importantly than the Cu ions from the octahedral symmetry (Figure 2), the CSM parameter for octahedral geometry is 1.98 instead of 0 for a perfect octahedral geometry.[81] The Mn1 atom chelates the two nitrogen atoms N7 and N14 of the bipyridyl unit with a bite angle of 74.94(14)°, and the N-Mn and O-Mn distances are in the ranges of 2.20-2.22 and 2.14-2.17 Å, respectively.

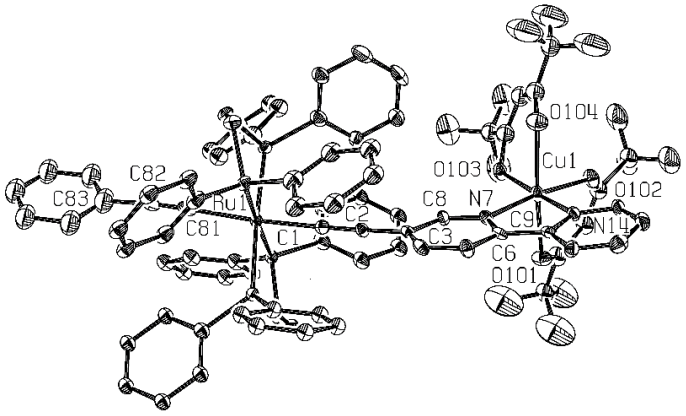

Figure 1. Perspective view of **1Cu**. Thermal ellipsoids are at the 50% probability level. Hydrogen atoms have been omitted for clarity.

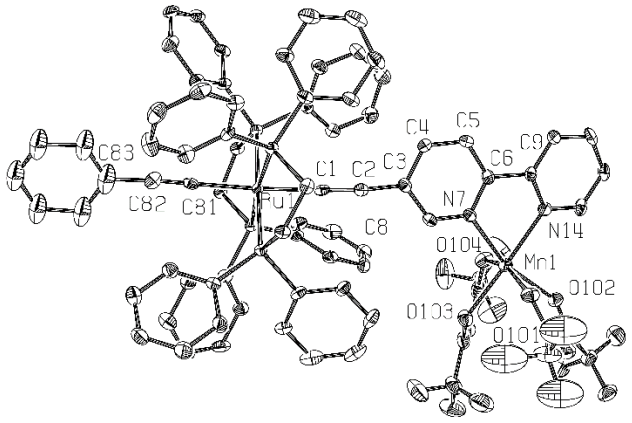

Figure 2. Perspective view of **1Mn**. Thermal ellipsoids are at the 50% probability level. Hydrogen atoms have been omitted for clarity.

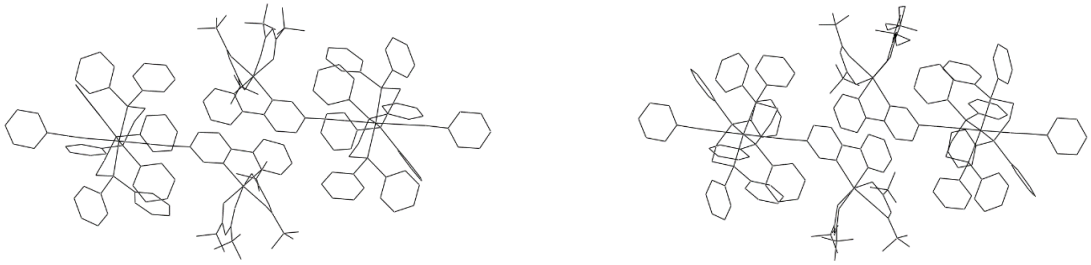

(a) (b)

Figure 3. Crystal packing in the solid state structures of (a) **1Cu** and (b) **1Mn**.

The two trimetallic complexes **2Cu** and **2Mn** are not isostructural but they both crystallize in the triclinic *P*-1 space group (Figure 4 and 5). The asymmetric unit includes one carbon-rich ligand and one $[M^{II}(hfac)_2]$ unit. The carbon-rich bonding between the ruthenium atom and the bipyridyl moieties is, here also, barely affected by the coordination, the angle between the pyridyl rings of the two parallel chelating bipyridyl (bipy) moieties being 1.18° for **2Cu** and 4.44° for **2Mn**. There is also extended π-

π stacking of the bipy systems characterized by inter-planar distances of 3.400 Å for **2Mn**, and 3.385 Å for **2Cu** (Figure 6). It is to be noted that because of this π-π stacking, inter-molecular metal-metal distances are much shorter than the intra-molecular ones, with 7.249 Å between the closest Mn atoms and 7.470 Å between the closest Cu ones for **2Mn** and **2Cu** respectively (to be compared to 16.725 and 16.578 Å for the Mn…Mn and Cu…Cu intramolecular distances respectively).

Concerning **2Mn**, the Mn atoms are six coordinated and the coordination sphere is very close to a trigonal prism (the CSM parameter being 0.31 for this geometry) (Figure 5). Indeed, as observed with **1Mn**, the Mn1 atoms chelate the two nitrogen atoms N7 and N14 of the bipy unit with a bite angle of 73.02°, and the N-Mn and O-Mn distances are in the ranges of 2.23-2.24 and 2.15-2.18 Å, respectively. Concerning **2Cu**, the Cu^{II} coordination is very similar to that observed in **1Cu** with distorted octahedral coordination geometries and warrants no further comment.

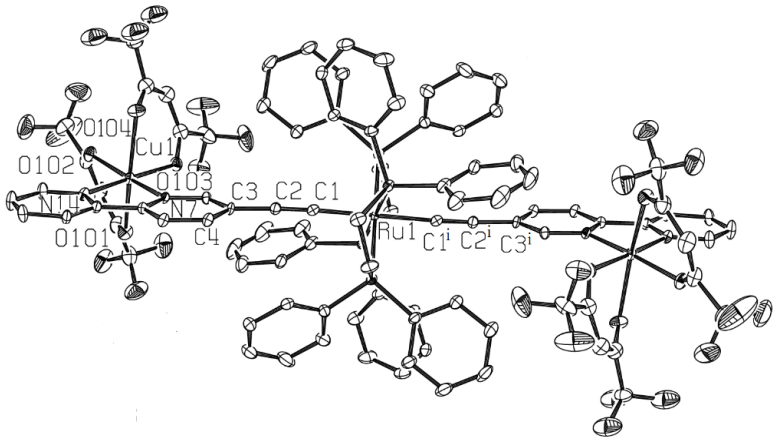

Figure 4. Perspective view of **2Cu**. Thermal ellipsoids are at the 50% probability level. Hydrogen atoms have been omitted for clarity.

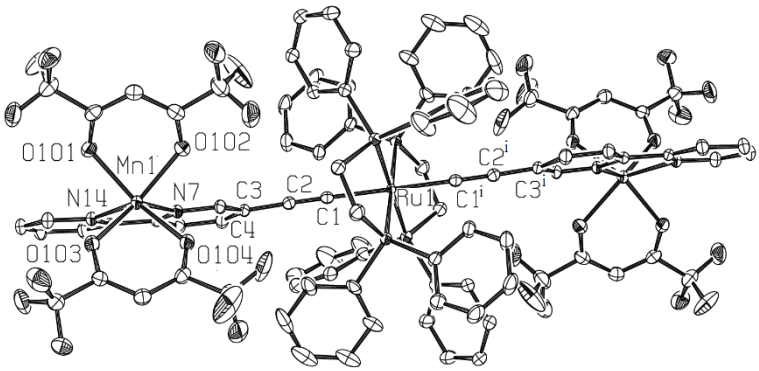

Figure 5. Perspective view of **2Mn**. Thermal ellipsoids are at the 50% probability level. Hydrogen atoms have been omitted for clarity.

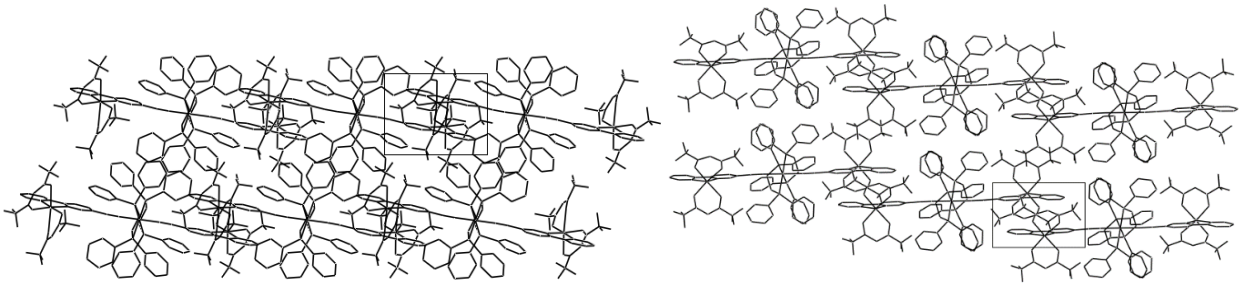

(a) (b)

Figure 6. Crystal packing in the solid state structures of (a) **2Cu** and (b) **2Mn**

Electrochemical data. Cyclic voltammetry traces (CVs) were recorded for all compounds to study the nature of their redox properties (CH_2Cl_2 solutions, 0.1 M Bu_4NPF_6). The values of the potentials are reported in Table 1, and the CV of **1Cu** is displayed in Figure 7. As expected, the bi- and tri-metallic complexes **1Mn,Cu** and **2Mn,Cu** display a first reversible redox process, as required for the desired switching event, at higher potentials than those of the parent complexes (E°= -0.009 and 0.078 V vs FcH^+/FcH for **1** and **2**, respectively)[21] as a result of the coordination of the electron withdrawing paramagnetic $M^{II}(hfac)_2$ units. This oxidation process is often erroneously viewed as essentially involving the Ru^{III}/Ru^{II} couple whereas it actually strongly involves the carbon-rich ligands to an extent depending on the nature of these ligands.[47, 82-85] Accordingly, in the present situation, the computational studies detailed below also show important changes in the distances of the acetylide units and spin-delocalization all along the conjugated path upon oxidation. In addition, for the copper derivative, it was observed an ill-defined irreversible redox wave at ca. -0.7/-0.8 V involving the $Cu(hfac)_2$ moieties (Table 1).[86]

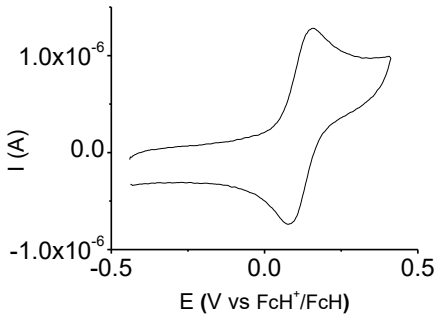

Figure 7. CV trace obtained for **1Cu** in CH_2Cl_2 (Bu_4NPF_6, 0.1 M); v = 100 $mV.s^{-1}$.

UV-vis-NIR and IR spectro-electrochemical studies. In addition to intense short-wavelength absorption bands for π–π* transitions involving the dppe ligands and the carbon-rich ligand (Intra-Ligand (IL) transitions), the polymetallic complexes show an absorption bands at λ_{max} = 468 nm and λ_{max} = 494 nm for the Mn and Cu adducts, respectively (Figure 8, Table 1). As we previously suggested,[21,75] this multi-configurational metal-to-ligand charge transfer (MLCT) might be the result of a charge transfer from Ru(dπ)/alkynyl based orbitals to a π* orbital based on the bipyridine unit, an assignment enforced by the marked bathochromic shift of Δλ = 62 - 96 nm (3260 - 4880 cm^{-1}) observed upon complexation of the parent ligand **1** and **2** displaying that transition at 398 and 406 nm, respectively. Indeed, such red shifts are characteristic of CT type transitions and are due to the enhancement of bipyridyl moieties electron withdrawing character upon further complexation.[87] Interestingly, the shift is similar whether the complex is coordinated to one or two paramagnetic metal(s). This further indicates that there is no direct electronic coupling between the two $M(hfac)_2$ units in the ground state. Note that the copper d-d transition of the copper units is probably hidden in the tail of the "MLCT" band.

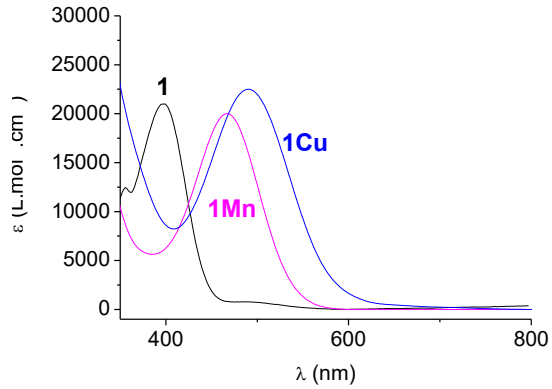

Figure 8. Electronic absorption spectra of **1** (black), **1Cu** (blue), and **1Mn** (magenta) in CH_2Cl_2.

As mentioned in the previous section, all compounds present a fast and reversible first oxidation process. Therefore, to collect experimental information about the oxidized species required for the switching events, their absorption properties upon oxidation/reduction were investigated by means of UV/Vis/NIR spectro-electrochemistry (SEC) in an optically transparent thin-layer electrochemical (OTTLE) cell (Table 1, Figure 9). The oxidation potential of the device was set between the first and

second oxidation potentials of each complex in order to perform oxidation of the organometallic core only, further oxidation being irreversible on the timescale of the experiments. Therefore, while the band located around 300 nm are slightly affected, one-electron oxidation of **1Cu,Mn** and **2Cu,Mn** mainly gives rise to the decrease of the band in the visible range to the benefit of a new broad absorption band in the NIR region of the spectrum at ca. 1040 nm, probably due to transitions from HOMO-n to the singly-occupied molecular orbital resulting from the depopulation of the HOMO dπ/π orbital, as previously observed for related complexes.[20, 21, 73] Interestingly, this broad band is similar for the four paramagnetic complexes, but a slight bathochromic shift is observed ($\Delta\lambda$ = 20 nm, ca. 150 cm^{-1}) when going from **1Cu,Mn**$^{+}$ to **2Cu,Mn**$^{+}$. A closer inspection of the energy plot of these NIR bands reveals that the shoulders result from the overlap of several transitions. They are consistent with observations reported by Low and co-workers[88] on others carbon-rich ruthenium acetylides who assigned such envelopes to the presence of different thermally accessible conformational structures due to relative orientations of the metal fragment and arylethynyl moieties, features also recently observed upon oxidation of the parent complexes bearing lanthanide ions or verdazyl/nitronyl-nitroxide units.[21, 73] With the copper complexes more than 90% of the intensities of the original spectra were recovered after reduction in the spectral region of interest, with no features other than those of the parent material. In contrast, **1Mn** and **2Mn** display only 60 to 75 % of the original intensities due to degradation for reasons that remain unclear so far. *Therefore, further experiments on Mn complexes were not considered.*

Additional IR experiments were conducted in the OTTLE cell with the Cu complexes. They show an expected shift of the asymmetrical $\nu_{C\equiv C}$ to smaller wavenumbers upon one electron removal (Table 1), i.e. from 2032 cm^{-1} to 1910 cm^{-1} for **1Cu** (Figure 10), due to the bond weakening of the acetylide linkages. Indeed, as reported in the theoretical section and in agreement with these IR band shifts, the C≡C distances are elongated by 0.005 Å in average upon oxidation for **1Cu** and, to a smaller extent, by 0.002 Å for **2Cu**. The Ru-C bonds are concomitantly shortened to a larger extent, 0.026 Å and 0.017 Å for **1Cu** and **2Cu**, respectively. Note the $\nu_{C=O}$ vibrations of the hfac ligands remain unaffected upon oxidation, a fact in line with the location of the oxidation on the carbon-rich moiety.

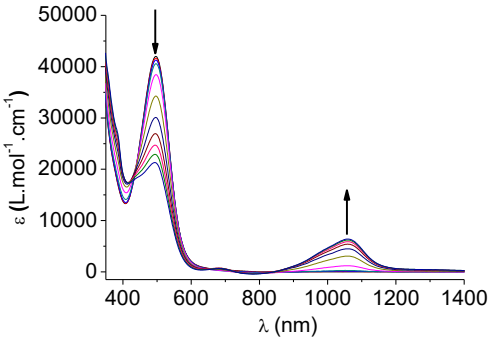

Figure 9. Electronic absorption spectra obtained upon the first oxidation of **2Cu** in an OTTLE cell (CH_2Cl_2, 0.2 M Bu_4NPF_6).

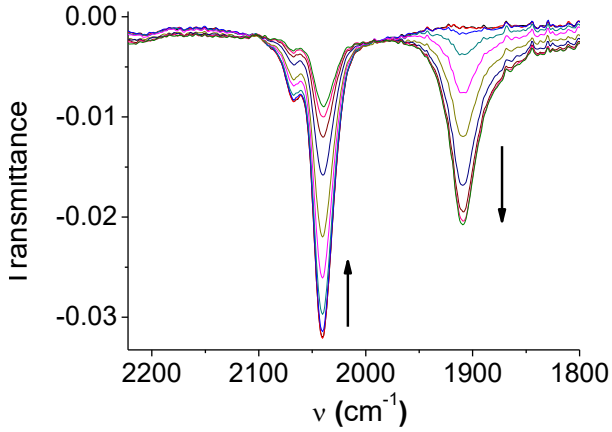

Figure 10. Spectroscopic changes observed in the IR region upon oxidation of **1Cu** to **1Cu**$^+$ in an OTTLE cell ($C_2H_4Cl_2$, 0.2 M Bu_4NPF_6).

Theoretical investigations, magnetic interactions, SQUID and EPR measurements. Interestingly, less than a hundred of magnetic studies of coordination chemistry compounds presenting three magnetic centers in a linear arrangement have been reported (see supporting information). The studies of the magnetic properties of this large variety of systems having in common to associate three magnetic units encompass the use of a spin Hamiltonian (See Eq. 1 and Chart 2) as the one originally proposed by Kambe[89] in 1950 where J_{ij} is the magnetic coupling between the ith and jth magnetic centers, *1*, *2* and *3* here, and $\hat{S}$ their spin operators:

$$\hat{H} = -\left[J_{12}\left(\hat{S}_1\hat{S}_2\right) + J_{23}\left(\hat{S}_2\hat{S}_3\right) + J_{13}\left(\hat{S}_1\hat{S}_3\right)\right] \quad (1)$$

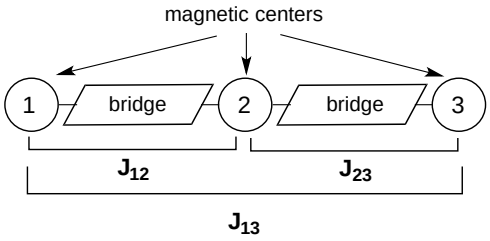

Chart 2

This Hamiltonian can be further improved by including zero-field splitting and other elements due to spin-orbit coupling and anisotropy as exemplified by the work of Lloret and collaborators on cobalt-containing systems.[90, 91] In these studies, the authors considered the magnetic coupling between the magnetic end-groups J_{13} as negligible. This hypothesis is justified by citing the work of Zhao and co-workers.[92] In this paper, the authors support their hypothesis by citing a work of Reedijk and co-workers of 1984, and the pioneering works of Sherwood and collaborators in 1968 and of Mackey and Martin in 1978 (see SI, Table S2-S3 as recent literature survey).[93-95]

In that context, one of the purposes of the present work being to study the influence of oxidation on the magnetic properties, an evaluation of the magnetic coupling between the terminal magnetic centers J_{13} concomitantly with J_{12} and J_{23} parameter is necessary. Indeed, the early works done in the sixties showed the drastic influence of the J_{12}/J_{23} over J_{13} parameter onto the magnetic response upon temperature[94] and the dilemma caused by the possibility of having several sets of parameters giving similarly-good fits of the magnetic experimental measurements.[95] Theoretical investigations of the magnetic interactions constitute an interesting tool to discriminate and provide its analysis in terms of electronic interactions. In some cases, intermolecular magnetic interactions have to be considered and in that case also a quantum chemical study was performed.[96]

Computation studies of **1Cu**, **1Cu**$^{+}$, **2Cu**, **2Cu**$^{+}$. Density functional (DFT) calculations are the only quantum chemical (QC) methods able to provide good approximation of magnetic couplings in such very large organometallic systems for which no ligand simplification was made. Full geometry optimizations with tight optimization criteria were performed for the four compounds using the X-Ray structures of **1Cu**, **2Cu** as guess geometries (see computational details). The Cartesian coordinates of all optimized structures are given in Table S5. The agreement between the experimental

structures and the optimized geometries of **1Cu**, **2Cu** (high-spin electronic configuration) is in the same range of deviation than that found in the literature for similar systems. The changes in the distances in the organic part is of less than 0.02 Å while, as usual, the metal-ligand distances are less well reproduced (deviations: 0.05 Å for Cu-O and 0.10 Å for Ru-P). The conformations between the $Ru(dppe)_2$ moiety and the $Cu(bpy)(hfac)_2$ were kept almost unchanged compared to the X-Ray structures of **1Cu** and **2Cu** (< 0.5 °). The optimized cationic geometries $\mathbf{1Cu}^+$ and $\mathbf{2Cu}^+$ (high-spin electronic configuration) show globally the similar geometrical changes compared to their neutral parents (see Table S4). The $Ru(dppe)_2(-C{\equiv}C)_2$ fragment is the most affected part of the molecules, in agreement with a ruthenium-centred oxidation in which the acetylide ligands is non-innocent.[5] The Ru-P distances are lengthened by 0.04 Å for **1Cu** and 0.05 Å for **2Cu** in average, while the Ru-C(≡C) are shortened in agreement with the bonding character of the HOMOs which are formally depopulated upon oxidation (-0.03 and -0.02 Å respectively). The rest of the distances are less affected but the more cumulenic character of the C≡C-C(aryl) chains has to be highlighted. Unfortunately, conformational studies of the cationic compounds could not be envisaged since several months of calculations are needed to attain a level of geometry and energy convergences necessary for magnetic investigations for each geometrical arrangement. Single point calculations were nevertheless performed in order to have indications on the expected energetics trends upon rotation of the end-fragments one compare to the other (see below).

Density functional theory (DFT) calculations using the broken-symmetry (BS) approach developed by L. Noodleman to calculate energies of spin eigenfunctions allows accessing to magnetic coupling values of the right order of magnitude (see Computational Details).[97]

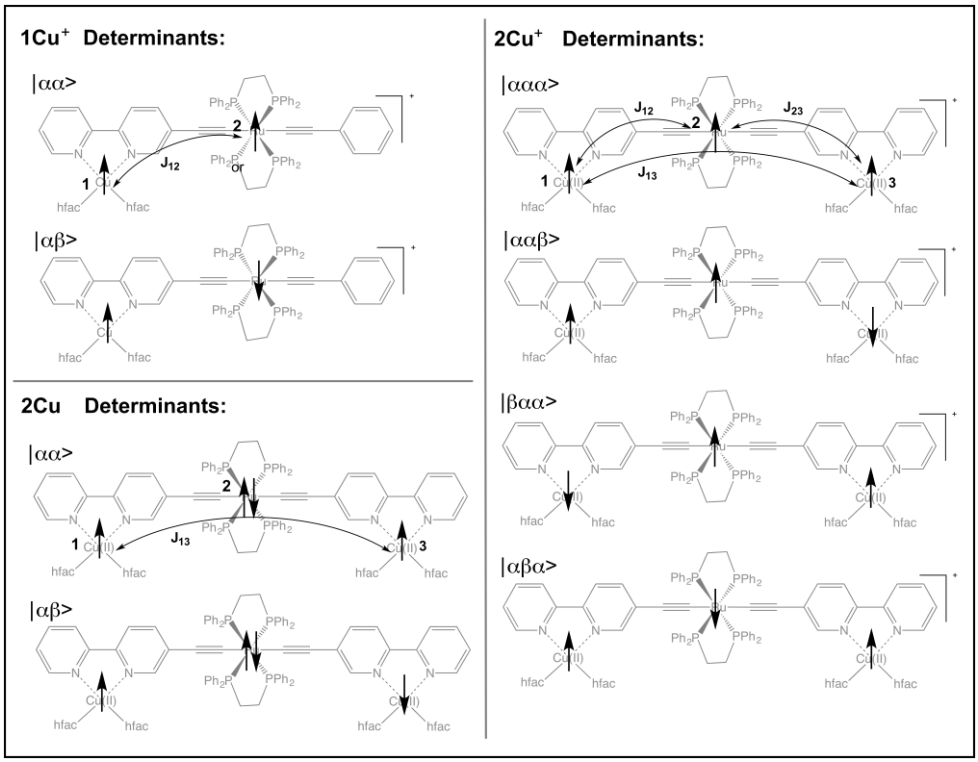

Scheme 2. Representation of the spin eigenfunctions and visualisation of the exchange coupling constants for **1Cu**+, **2Cu**$^{0/+}$.

The magnetic coupling between localized spins is usually described using a phenomenological Heisenberg Hamiltonian:

$$\widehat{H} = -\sum_{i,j} J_{ij}\, \widehat{S}_i \widehat{S}_j \qquad (2)$$

In systems with two magnetic centres **A** and **B**, the extraction of the magnetic parameter is well known. The exchange integral J is obtained using the two solutions |αα> and |αβ> (α = spin up, β = spin down):

$$E_{|\alpha\alpha\rangle} - E_{|\alpha\beta\rangle} = -J_{AB}/2 \qquad (3)$$

A key to a successful computation of J_{AB} with BS-DFT is an appropriate mapping between broken symmetry, high spin, and Heisenberg Hamiltonian states. In that sense, the spin contaminations in the broken symmetry solutions are important to consider. The spin eigenvalue basis set elements |αα>, |αβ> were computed for **1Cu**$^+$, **2Cu** (see Scheme 2 for the determinant description). The magnetic centres are in all cases S=1/2 localized being the Cu and Ru ions for **1Cu**$^+$ and the two Cu ions for the

2Cu. Eq 3 was applied to access the magnetic coupling J_{AB} using three different DFT functionals in order to evaluate a DFT uncertainty. The results are given in Table 3 and 4. For sake of comparison J_{13} was employed for **2Cu** considering the centre *2* (Ru) as non-magnetic. The influence of the atomic basis set (TZP vs DZP for the main group atoms) was evaluated for **1Cu**$^+$ in order to validate the use of the reduced TZP/DZP basis set for the trimetallic parents (vide infra).

Table 3. Calculated magnetic coupling J_{12} for **1Cu**$^+$ considering the magnetic centres *1* (Cu) and *2* (Ru) (see Scheme 2).

Atomic basis set	DFT functional	J_{12} (eV)	J_{12} (cm^{-1})
Ru/Cu: TZP All others: DZP	B3LYP	-0.0025	-20.4
	PBE0	-0.0022	-17.7
	M062X	-0.0008	-6.4
TZP for all	B3LYP	-0.0026	-21.0
	PBE0	-0.0022	-18.1

Table 4. Calculated magnetic coupling J_{13} for **2Cu** considering the magnetic centres *1* and *3* as being the Cu atoms (see Scheme 2).

DFT functional Basis set TZP	J_{13} (eV)	J_{13} (cm^{-1})
B3LYP	-0.0000	-0.1
PBE0	-0.0000	-0.2
M062X	-0.0000	-0.1

The spin contamination was evaluated for each |αα> and |αβ> solutions for each functional. The deviation of the calculated $\langle\widehat{S^2}\rangle$ from the theoretical value is within a range of +0.005 to +0.028 for the |αα> spin configuration and the BS solution |αβ>. For the latter, the value of $\langle\widehat{S^2}\rangle$ is 1, reflecting the ideal case of a BS solution intermediate between the spin states S = 1 and S = 3. The use of Eq. 3 is thus completely justified. The magnetic coupling J_{12} and J_{13} in **1Cu**$^+$ and **2Cu** respectively are of 14.8 ± 8.4 cm^{-1} and -0.1 ± 0.1 cm^{-1}.

The magnetic exchange of the hetero- tri-metallic system **2Cu**$^+$ can be tentatively analyzed via a valence-bond type of approach. This consists in considering ionic solutions in the strongly-correlated

Hubbard model using the so-called Stoner excitations[98] from the occupied spin-up to the unoccupied spin-down site:

$$\widehat{H}_h = \sum_{i\neq j,\sigma} t_{ij}.\left(c_{i\sigma}^{\dagger}.c_{j\sigma} + c_{j\sigma}^{\dagger}.c_{i\sigma}\right) + \sum_i U_i.n_{i\alpha}.n_{i\beta} - \sum_{i\neq j} K_{ij}.c_{i\alpha}^{\dagger}.c_{i\beta}.c_{j\beta}^{\dagger}.c_{j\alpha} \quad (4)$$

where t_{ij} are the hopping parameters, U the Hubbard Coulomb interaction and K, the direct exchange integral, for which the Hundt configurations are less favorable. The exchange integral J of the Heisenberg Hamiltonian can be expressed from this generalized Hubbard Hamiltonian, at the second order of perturbation:

$$J_{ij} = K_{ij} - 2t_{ij}^2/U \quad (5)$$

Two terms are in competition. The first one, K, leads to ferromagnetism but it rapidly decreases with the inter-spin distance. The second term, t^2/U, favors antiferromagnetism. Coming back to the examples reported in the literature gathered in Table S3, it is difficult to extract generalization considering the diversity of the nature of the magnetic interactions between first neighbors. Nevertheless, in all cases the magnetic exchange integral J_{13} between second neighbors *1* and *3* is always antiferromagnetic. Therefore, we can conclude that at a distance of more than 5.7 Å separating the magnetic centers *1* and *3*, K is small leading antiferromagnetic coupling issued from the t^2/U term of Eq 5. To evaluate the magnetic parameters using this approach, one needs to calculate electronic configuration that keeps the total charge of the system but with one magnetic center reduced and the other one oxidized. Unfortunately, we were unable to converge those configurations that are much higher in energy than the ground state.

To compute the magnetic exchange coupling, the Heisenberg-Dirac-Van Vleck (HDVV) Hamiltonian given in Eq. 1 was first employed. In that description, the eigenvalues are eigenstates of spin as detailed in SI (Eq S1-8). Unfortunately, the set of equations do not provide enough information to extract the three magnetic coupling constants J_{12}, J_{23} and J_{13} from the calculation of the spin determinant. Therefore, some approximations need to be made to obtain an estimation of the magnetic coupling between the first neighbors taking advantage of the geometrical characteristics of **2Cu**$^{+}$ and

the results already obtained for the bi-metallic analogues **1Cu**$^+$ and **2Cu**. Indeed, the two Cu magnetic centers are equivalent in **2Cu**$^+$. It is thus reasonable to consider $J_{12} = J_{23} = J$. We will do the assumption that magnetic interactions between second magnetic neighbors (Cu centers) are similar in the neutral and the oxidized systems even though slight geometrical changes are calculated. Indeed, J_{13} in **2Cu** is of roughly 0.1 cm^{-1} (see Table 4). It is thus reasonable to neglect this second neighbor interaction (hyp. $J_{13} = 0$). This lead to $E_Q - E_{D_1} = -\frac{3}{2}J$ (see SI Eq. S7). Using the computed energies of the (BS)-DFT calculations of the determinants |αβα>, |ααβ> and |βαα> for **2Cu**$^+$, we obtain the values given in Table 5 as function of the functional used. The computed value of J is of -12 ± 6 cm^{-1} at the considered optimized geometry of **2Cu**$^+$.

Table 5. Calculated magnetic coupling J for **2Cu**$^+$ considering a unique exchange integral J between first neighbours (HDVV Hamiltonian, hypotheses $J_{12} = J_{23}$ and $J_{13} = 0$)

DFT functional TZP(Ru/Cu)/DZP	J (eV)	J (cm^{-1})
B3LYP	-0.0015	-12.0
PBE0	-0.0022	-17.7
M062X	-0.0011	-9.2

A second resolution was recently proposed by Illas and coworkers.[99] It is based on the Ising model (approximation that all spins are oriented along the z-axis, see SI and Eq S9-17), and it was applied to the tri-metallic system **2Cu**$^+$. This methodology allows evaluating J_{13} that was neglected in the previous resolution. In that case again, the magnetic properties are calculated using the calculated energies of the spin eigenvalue basis set elements obtained from (BS)-DFT calculations (see Scheme 2).[100-102] These results are presented in Table 6. The basis set was decreased to a double-ζ STO atomic basis set for the main group atoms (see Computational Details), the calculation being too memory-demanding in this scheme of all-electron calculations. This lowering of atomic basis set was evaluated for **1Cu**$^+$ for which no noticeable effect on the magnetic coupling value was calculated (see Table 3).

Table 6. Calculated magnetic coupling J_{12}, J_{23}, J_{13} for **2Cu**$^{+}$ considering the magnetic centers *1* and *3* as being the Cu atoms and *2* the Ru one in the Ising level of approximation.

DFT functional TZP(Ru/Cu)/DZP	J_{12} (eV)	J_{12} (cm^{-1})	J_{23} (eV)	J_{23} (cm^{-1})	J_{13} (eV)	J_{13} (cm^{-1})
B3LYP	-0.0016	-12.7	-0.0014	-11.1	-0.0001	-0.5
PBE0	-0.0019	-15.7	-0.0024	-19.1	-0.0002	-1.5
M062X	-0.0011	-9.1	-0.0011	-8.7	-0.0001	-1.1

The Ising approach was applied to **2Cu**$^{+}$ using (BS)-DFT calculations to access to the energies of the determinants $|\alpha\beta\alpha>$, $|\alpha\alpha\beta>$ and $|\beta\alpha\alpha>$ lead to values of $J_{12} \simeq J_{23} = -13 \pm 6$ cm^{-1} and $J_{13} = -1 \pm 0.5$ cm^{-1} (deducted from Table 6). The hypotheses that $J_{13} = 0$ and $J_{12} = J_{23}$ made previously in the HDVV Hamiltonian resolution is confirmed. For strongly-correlated Hubbard model presented above, the Ising approach supports the argument that t^2/U favors antiferromagnetism that is mainly described by J_{13} magnetic exchange that is calculated ($J_{13} = -1 \pm 0.5$ cm^{-1} Ising model). This was predictable considering that **2Cu**$^{+}$ is the system for which the distance between *1* and *3* is the largest found in the literature (17.2 Å). Interestingly, even if small, J_{13} is roughly 10 times larger than in **2Cu** were the central Ru is not oxidized even if the distance between *1* and *3* is smaller (16.6 Å). This leads to conclude that the presence of spin localized of Ru in **2Cu**$^{+}$ increases the coupling between the Cu centers in that geometrical arrangement. On the contrary, J_{12} and J_{23} are 2 times smaller than J_{12} calculated for the parent **1Cu**$^{+}$. The oxidation that leads to an increase of the distance between the Cu *1* and *3* and the Ru atom *2* from 8.3 to 8.6 Å diminishes the magnetic interactions between neighboring magnetic centers. The metallic spin densities are of ±0.70 e for the copper atoms and ±0.70 e for Ru at the PBE0 level in the three configurations shown in Figure 11 (±0.66 e for Cu and ±0.64 e for Ru at B3LYP level; ±0.82 e for Cu and ±0.92 e for Ru at M062X level). The spin-density mapping plotted in Figure 11 nicely illustrates the magnetic interactions through a spin-polarization mechanism of almost the same extent whatever the functional used (0.41 to 0.46 e of total spin β for the $|\alpha\alpha\alpha>$ configuration, and 1.41 to 1.48 e of total spin β for the two others). The most stable spin eigenfunction $|\alpha\beta\alpha>$ that participates mostly to the magnetic coupling constant value J_{12} shows an important delocalization on the conjugated carbon ligand.

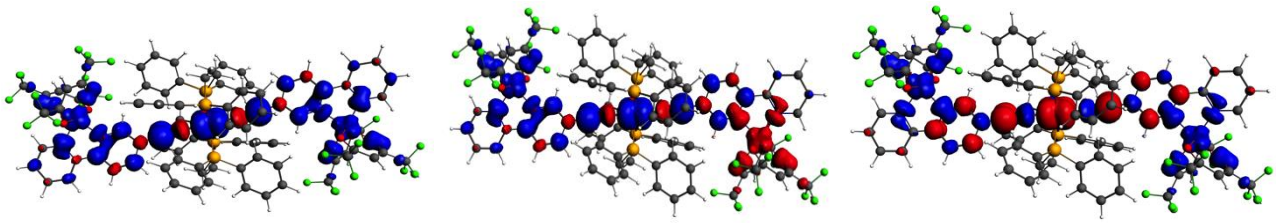

|ααα> |ααβ> |αβα>

Figure 11. Spin density iso-contour plots of **2Cu**$^{+}$ for the different calculated spin eigenfunctions; spin α in blue, spin β in red (TZP(Ru/Cu)/DZP / PBE0 level; similar maps are obtained with B3LYP and M062X functionals). Contour values: ± 0.0009 e/bohr^3. *

Considering the small values calculated for J_{13}, it was interesting to consider also the intermolecular magnetic couplings. Indeed, the π-π stacking observed in the crystal structures induces Cu···Cu intermolecular distances of 7.47 Å, much shorter than the intramolecular ones (16.58 Å). Considering the size of the systems, it was not possible to envision calculating a complete dimer. We choose to isolate two close packing Cu(bipy)(hfac)$_2$ in the **2Cu** crystal structures (all hydrogen atom positions were optimized). We have performed single point calculations of the triplet and the corresponding BS. In that case, only M062X functional was used since it better performs for non-covalent interactions (TZP atomic basis sets). The Cu spin densities are of ± 0.80 e close to the 0.82 e calculated for **2Cu** and **2Cu**$^{+}$ validating this approach. The difference in energy between two spin configurations is of 10^{-5} eV largely above the precision expected at that level of theory. In agreement with the experimental results in the solid state (see EPR section), we can thus conclude that the intermolecular magnetic interactions are negligible compared to the intramolecular ones even if the distances between the magnetic centers are two times shorter.

Finally, in order to evaluate the influence of the change of conformation that can occur in solution and evidenced by the NIR bands (vide supra), we performed sequential single point calculations for geometries in which one bipy plane was rotated compare the other bipy plane incrementally by 12° starting from the optimized geometry (the Cu(hfac)$_2$ coordination to the bpy was kept unchanged). Important steric hindrances were found between the hfac ligands and the dppe groups for most of the configurations since no geometry relaxation was performed. Only the conformers which total energy is less than 0.30 eV above the optimized structures were considered. Among them, the arrangement

presenting 72° between the pyridine planes show the largest magnetic difference with the optimized structures based on the X-Ray structures. In that case, the *J* value calculated for **2Cu**$^{+}$ is of -23.0 cm^{-1} using the procedure used to obtain values given in Table 5 at the M062X level for which -9.2 cm^{-1} was found for the optimized **2Cu**$^{+}$. Interestingly, the same geometry change was performed for **2Cu**. In that case, the initial J_{13} value of -0.1 cm^{-1} (Table 4, M062X level) representing the magnetic coupling between the Cu^{II} spin carriers for the optimized **2Cu** structure issued from the X-Ray arrangement is drastically enhanced by one order of magnitude to attain -1.6 cm^{-1}.

The DFT magnetic study of **2Cu** reveals that a small antiferromagnetic coupling exists via a spin polarized mechanism all along the conjugated path from one Cu^{II} end group to the other. It is sensitive to the conformation of the metallic fragments. Upon oxidation, the coupling between the Ru central unit and the Cu spin carriers is divided by two (from **2Cu** to **2Cu**$^{+}$).

EPR measurements of the neutral species. X-band EPR spectra of **1Cu** and **2Cu** complexes were recorded in diluted glassy CH_2Cl_2 solution. The spectrum recorded at 50 K depicted in Figure S2 for **1Cu** (see supporting information) is typical of mononuclear copper complex. The spin Hamiltonian parameters listed in Table 7 were obtained from the simulation of the EPR spectrum and show an approximatively axial symmetry for the *g* and *A* tensors. Further super hyperfine splitting is observed in the perpendicular part of the spectrum at ~330 mT due to the interaction of the unpaired electron with two equivalent nitrogen nuclei of the bipyridine ligand. These parameters are in good agreement with those obtained for closely related complexes with the copper embedded in a slightly distorted octahedral geometry.[103, 104] The EPR spectrum of binuclear complex **2Cu** shown in Figure 12 is different from the mononuclear complex **1Cu** with additional lines in the parallel component of the hyperfine tensor. The value of A_z is divided by two compared to the mononuclear complex and a transition is also observed at half field. These features are the signature of a thermally populated triplet state originating from an exchange-coupled pairs of Cu(II) ions. Therefore, in the parallel region ~ 330 mT, two septets which are shifted by the zero-field-splitting *D* could be observed. The spin Hamiltonian parameters (Table 7) deduced from the simulation provide a *D* value less than 0.003 cm^{-1} which lead to an overlap between two sets of seven lines.

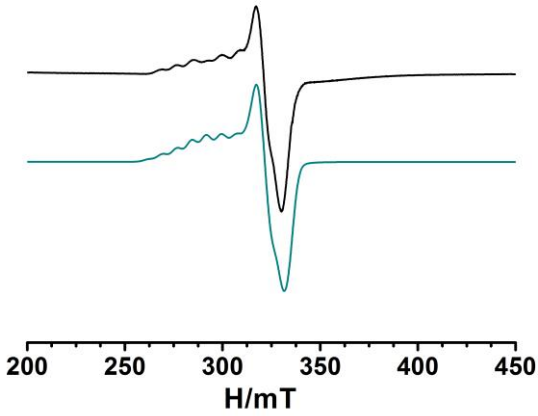

Figure 12. EPR spectrum of **2Cu** in CH_2Cl_2 at 4 K: upper trace, experimental signal; lower trace, simulated spectrum

Table 7. EPR parameters, *g* tensors and *A* hyperfine coupling constants in MHz, for **1Cu** and **2Cu** complexes in CH_2Cl_2 at 4 K.

	g_x	g_y	g_z	$A_x(^{63}Cu)$	A_y (^{63}Cu)	A_z (^{63}Cu)
1Cu	2.043	2.054	2.275	25	28	490
2Cu	2.027	2.098	2.334	15	15	250

Magnetic susceptibility measured by SQUID for **1Cu** and **2Cu** complexes have been obtained on polycrystalline sample in the [2-300 K] temperature range. The χT *vs* T plots are displayed in Figure S3 in supporting information. χT values of 0.4354 ± 0.0042 emu.K.mol^{-1} and 0.8288 ± 0.0008 emu.K.mol^{-1} were obtained at 300 K for **1Cu** and **2Cu** complexes respectively, close to the expected theoretical values for one and two isolated S=1/2 Cu(II) spins in such axial geometry. Due to the large intramolecular distance between the remote Cu(II) ions (16.58 Å), the **2Cu** complex exhibits an almost pure Curie behavior with a small upturn at low temperature indicative of very weak intermolecular interactions (J_{13}/k_B ~ -0.2 cm^{-1}).

The temperature dependence of the doubly integrated EPR signal of **2Cu** complex in frozen solution was also measured and plotted as $\chi_{EPR}T$ *vs* T (Figure S4). The magnetic data for **2Cu** were fitted using Bleaney-Bowers equation for two spins S=1/2:

$$\chi_{ST}(T) = \frac{2Ng^2\mu_B{}^2}{3k_BT} x \left[\frac{3}{3+\exp(-J/k_BT)} \right] \quad (6)$$

where μ_B and k_B are the Bohr Magneton and the Boltzmann constant respectively. Such behavior is consistent with two spins S=1/2 antiferromagnetically coupled with a value of J_{13}/k_B close to -7 K (-4.8 cm^{-1}). Since the solid state magnetic properties do not reveal such intramolecular magnetic interaction as predicted by calculations, we can conclude that the average molecular conformation have a significant impact on the magnetic coupling (see theoretical part and NIR spectroscopy) in solution as compared to the powder. Moreover, it points to the efficient indirect exchange pathway through the polarization of the Ru orbitals. In the absence of aggregation phenomena, the low concentration of the solution (10^{-4} M) ensures the measurement of the magnetic properties of **2Cu** through EPR corresponds to the one of isolated molecules and it thus originates from an intramolecular interaction. Note that the computational studies reveal also that even if the intermolecular Cu-Cu distances are shorter than the intramolecular ones (7.47 Å compared to 16.48 Å in **2Cu**) it does not increase magnetic interactions.

EPR measurements of the oxidized systems. Chemical oxidations by $KAuCl_4$ in CH_2Cl_2 were performed on compounds **1Cu** and **2Cu** and followed by recording UV-visible and EPR spectra. One-electron oxidation of **1Cu** and **2Cu** leads to the same UV-visible spectra obtained by spectro-electrochemistry (see Figure S5 and S6). At low temperature, the shape of the EPR spectra of **1Cu**$^+$ and **2Cu**$^+$ are almost identical to that of the neutral species. Only the enhancement of intensity proves the addition of spins on the molecule (Figure S7). The EPR signal of the oxidized species is probably isotropic with a *g* value close to 2.00 as already observed for other Ru complexes[105] and masked by the perpendicular component of the EPR spectrum of copper. The temperature dependence of the doubly integrated EPR signal χ_{EPR} was also measured. The line shapes of the EPR signal are not affected by temperature so we reported the peak-to-peak amplitude $A_{pp}T$ *vs* T. The product of $A_{pp}T$ *vs* T for **1Cu**$^+$ complex is reported in Figure 13. It can be reproduced by the sum of the two contributions

according to Equation 7, where the first and second terms represent the contributions from (i) the Curie law χ_{Curie} and (ii) the singlet-triplet system $\chi_{ST}(T)$:

$$\chi(T) = x\chi_{Curie}(T) + (1-x)\chi_{ST}(T) \quad (7)$$

In this equation, we have taken into account a proportion of the non-oxidized species *x* for which the doubly integrated signal is assumed to follow the Curie law. Three experiments were recorded with different *x* values estimated from the UV-visible spectra and A_{pp} values were normalized to the value x=0.68. Thus, the best fit parameter gives J_{12}/k_B = -8.0 K ± 0.5 K (-5.6 cm^{-1}) thus pointing towards a singlet ground state. However, the fitting is very sensitive to the *x* parameter. If the two parameters J/k_B and *x* are free we found J/k_B = -16.0 K ± 1.5 K (-11.1 cm^{-1}) and *x* = 0.75 to be compared to the above experimental value of 0.68.

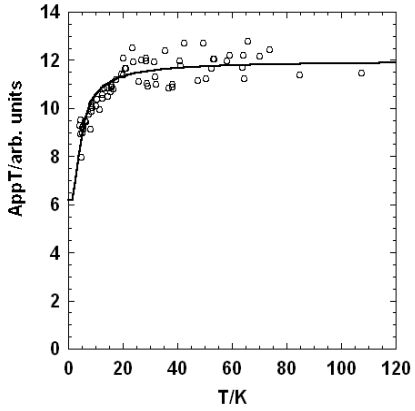

Figure 13. Temperature dependence of the EPR susceptibility (given by $A_{pp}T$ product*)* in CH_2Cl_2 solution for **1Cu**$^+$ complex.

The same experiment was performed for **2Cu**$^+$ complex and the UV-visible spectra evolution were recorded to follow the oxidation steps. Similar results are obtained by spectro-electrochemistry. They clearly indicate the presence of the oxidized species. Few changes are observed on the EPR spectrum at low temperature and the presence of an additional spin on the molecule is deduced from the increase of the EPR intensity. The analysis of the experimental $A_{pp}T$ *vs* *T* is performed according to Equation 8. As suggested by DFT calculations, the J_{13} value between the remote Cu spin carriers within a linear 3-spins model is negligible. The theoretical computations additionally suggest that the Ru-Cu exchange interactions J_{12} and J_{23} are almost identical, allowing to consider a unique Ru-Cu exchange

coupling, *J*. The experimental difficulties related to the incomplete oxidation in the EPR experimental conditions introduce an additional parameter as the concentration of non-oxidized complex. The suggested simplification of the interaction scheme by the theoretical discussion allows thus avoiding over-parameterization of the data fitting procedure. In Equation 8, J_{3S} represents the doublet-quartet and J_{ST} the singlet-triplet splitting respectively, whereas C is the Curie constant.

$$\chi_{ox}T = C\left\{x\left(\frac{3x}{3+\exp(-\Delta_1)}\right)+(1-x)\left[\frac{10+\exp(-3\Delta_2)+\exp(-\Delta_2)}{2+\exp(-3\Delta_2)+\exp(-\Delta_2)}\right]\right\} \quad \chi_{3S}(T)=\frac{C}{T}\left[\frac{10+\exp(-3J_{3S}/k_BT)+\exp(-J_{3S}/k_BT)}{2+\exp(-3J_{3S}/k_BT)+\exp(-J_{3S}/k_BT)}\right] \quad (8)$$

$$\Delta_1 = J_{ST}/k_BT\,;\ \Delta_2 = J_{3S}/k_BT$$

We have taken into account a proportion of non-oxidized species *x* for which the χ_{EPR} is assumed to follow a Bleaney-Bowers law. The fitting was performed with the value of J_{ST}/k_B=-7 K previously determined from EPR data and a *x* value of 0.4 extracted from UV-visible data. Least-squares fitting of J_{3S}/k_B value gave a value of -3.5 ± K (-2.4 cm $^{-1}$). We also checked that the variation of J/k_B and/or *x* ratio did not dramatically change the J_{3S} value. J_{3S}/k_B were spread between -2.5 K and -3.4 K when J_{ST}/k_B varies between -10 K to -2 K with *x* = 0.4. The *x* ratio was also varied between 0.1 to 0.9 with J_{ST}/k_B= -7 K and J_{3S}/k_B spreads between -2.4 K to -3.5 K.

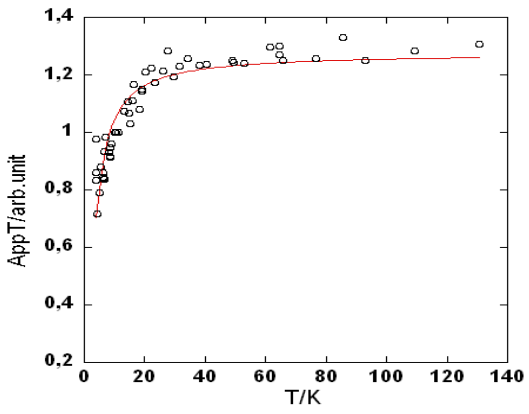

Figure 14. Temperature dependence of the product $A_{pp}T$ in CH_2Cl_2 solution for **2Cu**$^+$ complex.

As already observed the value of J_{ST}/k_B exchange coupling decreases when the distance between the two spin carriers increases and the values are close to zero for systems separated by metal such as Pt with phenyl ethylene as spacers.[72] The J_{ST}/k_B exchange coupling for the **2Cu** neutral complex of -

7 K (-4.8 cm^{-1}) is relatively high for this system where the two spins carriers are separated by a distance of 16.6 Å. This is in favor of the ability of diamagnetic ruthenium to operate as connector for magnetic exchange between carbon rich ligand *via* a spin polarization mechanism along the conjugated ligands as revealed by DFT calculations. It also results from the presented study that similar trends are deduced for the magnetic exchange couplings calculated at DFT level or assessed through EPR experiments in term of nature and order of magnitude. Concerning this **2Cu** complex, the experimental coupling (EPR) of -4.8 cm^{-1} between the two Cu spin carriers is thus consistent with DFT prediction of -0.1 to -1.6 cm^{-1} taking into account different possible conformations in (frozen) solution (vide supra). The relevance of this conformation factor is enforced by the observation of a weaker coupling in solid state observed by SQUID measurements (-0.2 cm^{-1}), where additional interactions can also occur (vide supra).

For the oxidized species and $\mathbf{1Cu}^{+}$, DFT calculations predict an antiferromagnetic coupling between Cu and the oxidized ruthenium center of -14.8 ± 8 cm^{-1}. This is also consistent with the experimental EPR values of -5.8 to -11.1 cm^{-1}, taking into account the effect of a slight variation on the precision of the estimated amount of non-oxidized **1Cu**. With **2Cu**, DFT predict a value of -13 ± 6 cm^{-1} to be compared to -2.4 cm^{-1} (best EPR fit). Here again, the conformation in frozen solution with respect to an optimized structure is a crucial point. Indeed, the calculated magnetic coupling can be divided by 3 (on the example of one functional, vide supra) depending on the conformers which gives a reasonable agreement between experiment and theory. Unfortunately, a complete conformational study that would give a clear picture is not possible so far (size of the systems). Finally, it is worth noting that the significant decrease of the magnetic coupling upon oxidation of **2Cu** with respect to the neutral species is an unusual phenomenon previously observed to a lesser extent with nitronyl-nitroxide and verdazyl radicals,[73] due to an incoming predominant interaction issued from the novel delocalized ruthenium spin carrier. Its lower amplitude is ascribable to conformational issues difficult to rationalize on the basis of actual theory limitations.

Conclusion. In this work, we have synthesized a new series of ruthenium complexes bearing paramagnetic Cu^{II} and Mn^{II} metal centers. All of these complexes have been characterized by X-ray structural determinations. They oxidize readily and reversibly in the CV experiments but the spectroelectrochemical studies show that only the copper system is well suited to achieve redox switches. SQUID, EPR spectroscopy studies and computational studies reveal that an antiferromagnetic coupling exists in **2Cu** although a large distance is separating the spin carriers (16.6 Å). It benefits from the efficient conjugated path that includes a Ru center that mediates magnetic coupling via a spin polarized mechanism. Oxidation modifies importantly this coupling by creating a third spin carrier within the conjugated path localized on the $Ru(-C\equiv C-)_2$ central part. In that case, the magnetic interaction is now largely dominated by the lower antiferromagnetic coupling between this spin carrier and the Cu^{II} end groups, which is an unusual phenomenon. Interestingly, one electron oxidation of **1Cu** generates an interaction between the Cu^{II} and Ru spin carriers of comparable magnitude to that observed between the two far apart Cu^{II} ions in **2Cu**. All these results were rationalized by DFT calculation concomitantly using a Heisenberg-Dirac-Van Vleck Hamiltonian and an Ising model. Importantly, this work demonstrates that a precise molecular engineering can offer means to modify magnetic properties using the redox ability of incorporated units. Besides, further functionalization of such systems offers an enhanced potential for increased functionality.

Acknowledgments: We thank the Université de Rennes 1, the CNRS, the ANR (RuOxLux - ANR-12-BS07-0010-01), and the Région Bretagne (PhD grant for EDP) for support. Computations were performed using HPC resources from GENCI-CINES/IDRIS (Grants 2014-17/80649). C. B. also acknowledge the Narodowe Centrum Nauki (Poland) for its support via a SONATA project (UMO-2015/17/D/ST3/00883).

Supporting Information Available: General considerations concerning magnetic properties in linear trinuclear systems. Additional UV-visible, electrochemical and magnetic data, cif files, cartesian coordinates of the DFT optimized structures. This material is available free of charge via the Internet at for this article is available on the www under http://pub.acs.org.

EXPERIMENTAL SECTION

General comments: The reactions were carried out under an inert atmosphere using Schlenk techniques. Solvents were dried and distilled under argon using standard procedures. The ruthenium complexes **1** and **2** have been obtained as previously reported.[20, 21] High resolution mass spectra (HRMS) were recorded in Rennes at the CRMPO (Centre Régional de Mesures Physiques de l'Ouest) on a ZabSpecTOF (LSIMS at 4 kV) spectrometer.

Electrochemical studies were carried out under argon using an Eco Chemie Autolab PGSTAT 30 potentiostat (CH_2Cl_2, 0.1M Bu_4NPF_6), the working electrode was a Pt disk, and ferrocene the internal reference.

UV-vis-NIR spectroelectrochemistry (SEC) experiments were performed at 20 °C, under argon, with a home-made Optically Transparent Electrosynthetic (OTE) cell, path length = 1 mm, using a Varian CARY 5000 spectrometer and an EG&G PAR model 362 potentiostat. A Pt mesh was used as the working electrode, a Pt wire as the counter electrode, and an Ag wire as a pseudo-reference electrode. The electrodes were arranged in the cell such that the Pt mesh was in the optical path of the quartz cell. The anhydrous freeze-pump-thaw degassed sample-electrolyte solution (0.2 M *n*-Bu_4NPF_6 in dichloromethane) was cannula-transferred under argon into the cell previously thoroughly deoxygenated. IR experiments were performed in similar conditions with dichloroethane as the solvent, using a modified cell with KBr windows, and a Bruker IFS28 spectrometer.

EPR spectra were recorded on a Bruker EMX spectrometer operating at X-band (9.4 GHz) with a standard rectangular cavity (TE 102). An ESR900 cryostat (Oxford Instruments) was used for the low temperature measurements. Sample solutions (10^{-4} M) in quartz tubes were degassed by three freeze-and-thaw cycles. Single oxidized species were generated by addition of 1 eq. $KAuCl_4$ in glovebox. Simulation of spectra were performed with Easyspin program package described by Stoll and Schweiger.[106]

The XRD data have been measured on a APEXII, Bruker-AXS diffractometer at Mo-Kα radiation (λ = 0.71073 Å). The structures were solved by direct methods using the SIR97 program,[107] and then

refined with full-matrix least-square methods based on F^2 (SHELX-97)[108] with the aid of the WINGX program.[109] The contribution of the disordered solvents to the calculated structure factors was estimated following the BYPASS algorithm,[110] implemented as the SQUEEZE option in PLATON.[111] A new data set, free of solvent contribution, was then used in the final refinement. All non-hydrogen atoms were refined with anisotropic atomic displacement parameters. H atoms were finally included in their calculated positions. CCDC deposition numbers for the four complexes are 1466553-6.

Polymetallic complexes – General procedure. $[M^{II}(hfac)_2].2H_2O$ and the ruthenium complex (**1** or **2**) were dried under vacuum for 30 min, then dissolved in CH_2Cl_2 (30 mL). The solution was stirred at ambient temperature for 4 hours, and a progressive precipitation of a solid from the solution is observed. The mixture was then taken to dryness under vacuum. The residue was washed with pentane (2 × 10 mL) and recrystallized from 1:2 CH_2Cl_2/pentane to yield the product as crystals.

***trans*-[Ph-C≡C-(dppe)$_2$Ru-C≡C-bipyCu(hfac)$_2$] (1Cu):** following general procedure, $[[Cu^{II}(hfac)_2].2H_2O$ (42.25 mg, 0,085 mmol) and **1** (100 mg, 0.085 mmol) in CH_2Cl_2 (30 mL) yielded to dark red crystals (98 mg, 0.060 mmol, 70%); IR (KBr, cm^{-1}): $\upsilon_{C\equiv C}$ 2031 (s), $\upsilon_{C\equiv O}$ = 1668; UV-vis (CH_2Cl_2) λ (nm) [ε mol^{-1} L cm^{-1}]: 494 [21000]. FAB^+-MS (CH_2Cl_2): *m/z* 1448.1928 $[M - hfac]^+$ (calculated 1448.19272)

***trans*-[Ph-C≡C-(dppe)$_2$Ru-C≡C-bipyMn(hfac)$_2$] (1Mn):** following general procedure, $[Mn^{II}(hfac)_2].2H_2O$ (39.87 mg, 0.085 mmol) and **1** (100 mg, 0.085 mmol) in CH_2Cl_2 (30 mL) yielded to orange crystals (77 mg, 0.047 mmol, 55%); IR (KBr, cm^{-1}): $\upsilon_{C\equiv C}$ 2042 (s), $\upsilon_{C\equiv O}$ = 1647; UV-vis (CH_2Cl_2) λ (nm) [ε mol^{-1} L cm^{-1}]: 468 [19000]. FAB^+-MS (CH_2Cl_2): *m/z* 1647.1939 $[M]^+$ (calculated 1647.18925)

***trans*-[(dppe)$_2$Ru(-C≡C-bipyCu(hfac)$_2$)$_2$] (2Cu):** following general procedure, $[Cu^{II}(hfac)_2].2H_2O$ (42.25 mg, 0.085 mmol) and **2** (53.38 mg, .,043 mmol) in CH_2Cl_2 (30 mL) yielded to dark red crystals

(90.64 mg, 0.043 mmol, 95%); IR (KBr, cm^{-1}): $\upsilon_{C\equiv C}$ 2030 (s), $\upsilon_{C\equiv O}$ = 1670; UV-vis (CH_2Cl_2) λ (nm) [ε mol^{-1} L cm^{-1}]: 494 [42000]. FAB$^+$-MS (CH_2Cl_2): *m/z* 2003.1281 $[M - hfac]^+$ (calculated 2003.12027)

***trans*-[(dppe)$_2$Ru(-C≡C-bipyMn(hfac)$_2$)$_2$] (2Mn):** following general procedure, $[Mn^I(hfac)_2].2H_2O$ (39.87 mg, 0.085 mmol) and **2** (53.38 mg, 0,043 mmol) in CH_2Cl_2 (30 mL); to give orange crystals (56.60 mg, 0.026 mmol, 60%); IR (KBr, cm^{-1}): $\upsilon_{C\equiv C}$ 2042 (s), $\upsilon_{C\equiv O}$ = 1649; UV-vis (CH_2Cl_2) λ (nm) [ε mol^{-1} L cm^{-1}]: 468 [25500]. FAB$^+$-MS (CH_2Cl_2): *m/z* 2194.1357 $[M]^+$ (calculated 2194.12524)

Computational details. Density functional theory (DFT) calculations were performed using the Amsterdam Density Functional package (ADF 2014.02) in order to better understand the electronic properties of the studied compounds.[112-114] Considering that magnetic properties are evaluated, we choose to keep the systems unmodified (no simplification of ligands) and not to impose symmetry constraint. This leads to large calculations with up to 205 atoms for which conformational studies are too resource demanding to be performed. The convergence criteria for the geometry optimizations starting from the available X-Ray structures (or parent redox structure) were more drastic than default ones (energy change < 0.0001 u.a., atomic position displacement < 0.001 Å). For geometry optimizations, electron correlation was treated within the local density approximation (LDA) in the Vosko-Wilk-Nusair parametrization.[115] The non-local corrections (GGA) of Becke and Perdew (BP86) were added to the exchange and correlation energies, respectively.[116, 117] The analytical gradient method implemented by Versluis and Ziegler was used.[118] Spin unrestricted calculations were performed for all the open-shell systems considered. We used the triple-ζ Slater Type Orbital (STO) basis set, TZP, provided by ADF program set with a medium frozen core (up to 1s for C and N, 2p for P, and 4p for Ru). The triple-ζ STO atomic basis set is augmented with a 2p polarization function for H, a 3d polarization function for C, N and P, and a 5p polarization function for Ru. We have used two (meta-)hybrid functional, B3LYP,[115, 116, 119, 120] PBE0[121, 122] and one meta-hybrid functional M06-2X[123, 124] to evaluate magnetic coupling constants. In that case, an all-electron basis set was necessary.

An all-electron TZP was used for **1Cu**$^{+}$ and compared to a mixed all electron TZP/double-ζ STO (DZP) (TZP for Cu and Ru atoms/ DZP for main group atoms). Energies of some spin eigenfunctions were obtained using the broken-symmetry (BS) approach developed by L. Noodleman.[97] Molecular orbitals and spin density were plotted with the ADF-GUI package.[125] The calculations of the excitation energies were intended in order to rationalize the optical properties of the studied systems. Geometry optimizations taking into account solvent effects (COSMO) using the B3LYP functional (see Cartesian Coordinated of the optimized structures in SI) followed by time-dependant DFT (B3LYP) were attempted. Unfortunately, we faced computational limitations (memory limitation in French High-computing Centers).

SYNOPSIS TOC

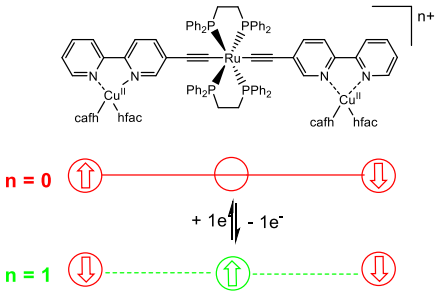

Ruthenium acetylide central unit sets up an antiferromagnetic coupling between two remote Cu^{II} spin carriers (16.6 Å) via a spin-polarization mechanism. Oxidation of this center modifies importantly this coupling by creating a third spin carrier and a new magnetic interaction largely dominated by the lower antiferromagnetic coupling between this spin carrier and the Cu^{II} end groups.

References.

1. Molecular Switches. In Feringa, B. L., Browne, W. R., Eds. Wiley-VCH, Weinheim, Germany: 2011.
2. *Spin-Crossover Materials: Properties and Applications*. Wiley-VCH, Weinheim: 2011.
3. Erbas-Cakmak, S.; Leigh, D. A.; McTernan, C. T.; Nussbaumer, A. L. Artificial Molecular Machines. *Chemical Reviews* **2015,** 115, 10081-10206.
4. de Silva, A. P. Molecular Logic Gate Arrays. *Chemistry-an Asian Journal* **2011,** 6, 750-766.
5. Costuas, K.; Rigaut, S. Polynuclear carbon-rich organometallic complexes: clarification of the role of the bridging ligand in the redox properties. *Dalton Transactions* **2011,** 40, 5643-5658.
6. Aguirre-Etcheverry, P.; O'Hare, D. Electronic Communication through Unsaturated Hydrocarbon Bridges in Homobimetallic Organometallic Complexes. *Chemical Reviews* **2010,** 110, 4839-4864.

7. Zalis, S.; Winter, R. F.; Kaim, W. Quantum chemical interpretation of redox properties of ruthenium complexes with vinyl and TCNX type non-innocent ligands. *Coordination Chemistry Reviews* **2010,** 254, 1383-1396.
8. Low, P. J. Twists and turns: Studies of the complexes and properties of bimetallic complexes featuring phenylene ethynylene and related bridging ligands. *Coordination Chemistry Reviews* **2013,** 257, 1507-1532.
9. Halet, J.-F.; lapinte, C. Charge delocalization vs localization in carbon-rich iron mixed-valence complexes: A subtle interplay between the carbon spacer and the (dppe)Cp*Fe organometallic electrophore. *Coordination Chemistry Reviews* **2013,** 257, 1584-1613.
10. Tanaka, Y.; Ishisaka, T.; Inagaki, A.; Koike, T.; Lapinte, C.; Akita, M. Photochromic Organometallics with a Dithienylethene (DTE) Bridge, Y-C≡C-DTE-C≡C-y (Y = {MCp*(dppe)}): Photoswitchable Molecular Wire (M = Fe) versus Dual Photo- and Ellectrochromism (M = Ru). *Chemistry-a European Journal* **2010,** 16, 4762-4776.
11. Lissel, F.; Fox, T.; Blacque, O.; Polit, W.; Winter, R. F.; Venkatesan, K.; Berke, H. Stepwise Construction of an Iron-Substituted Rigid-Rod Molecular Wire: Targeting a Tetraferra-Tetracosa-Decayne. *Journal of the American Chemical Society* **2013,** 135, 4051-4060.
12. Gauthier, N.; Olivier, C.; Rigaut, S.; Touchard, D.; Roisnel, T.; Humphrey, M. G.; Paul, F. Intramolecular optical electron transfer in mixed-valent dinuclear iron-ruthenium complexes featuring a 1,4-diethynylaryl spacer. *Organometallics* **2008,** 27, 1063-1072.
13. Green, K.; Gauthier, N.; Sahnoune, H.; Halet, J.-F.; Paul, F.; Fabre, B. Covalent Immobilization of Redox-Active Fe(kappa(2)-dppe)(eta(5)-C5Me5)-Based pi-Conjugated Wires on Oxide-Free Hydrogen-Terminated Silicon Surfaces. *Organometallics* **2013,** 32, 5333-5342.
14. Grelaud, G.; Cifuentes, M. P.; Paul, F.; Humphrey, M. G. Group 8 metal alkynyl complexes for nonlinear optics. *Journal of Organometallic Chemistry* **2014,** 751, 181-200.
15. Mulas, A.; Hervault, Y.-M.; He, X.; Di Piazza, E.; Norel, L.; Rigaut, S.; Lagrost, C. Fast Electron Transfer Exchange at Self-Assembled Monolayers of Organometallic Ruthenium(II) sigma-Arylacetylide Complexes. *Langmuir* **2015,** 31, 7138-7147.
16. Mulas, A.; Hervault, Y.-M.; Norel, L.; Rigaut, S.; Lagrost, C. Electron-Transfer Kinetics in Polymetallic Carbon-Rich Ruthenium(II) Bis(sigma-arylacetylides) Wires Connected to Gold. *Chemelectrochem* **2015,** 2, 1799-1805.
17. Malvolti, F.; Rouxel, C.; Triadon, A.; Grelaud, G.; Richy, N.; Mongin, O.; Blanchard-Desce, M.; Toupet, L.; Razak, F. I. A.; Stranger, R.; Samoc, M.; Yang, X.; Wang, G.; Barlow, A.; Cifuentes, M. P.; Humphrey, M. G.; Paul, F. 2,7-Fluorenediyl-Bridged Complexes Containing Electroactive "Fe(eta(5)-C5Me5)(kappa(2)-dppe)C C-" End Groups: Molecular Wires and Remarkable Nonlinear Electrochromes. *Organometallics* **2015,** 34, 5418-5437.
18. Samoc, M.; Gauthier, N.; Cifuentes, M. P.; Paul, F.; Lapinte, C.; Humphrey, M. G. Electrochemical switching of the cubic nonlinear optical properties of an aryldiethynyl-linked heterobimetallic complex between three distinct states. *Angewandte Chemie-International Edition* **2006,** 45, 7376-7379.
19. Green, K. A.; Cifuentes, M. P.; Samoc, M.; Humphrey, M. G. Metal alkynyl complexes as switchable NLO systems. *Coordination Chemistry Reviews* **2011,** 255, 2530-2541.
20. Di Piazza, E.; Norel, L.; Costuas, K.; Bourdolle, A.; Maury, O.; Rigaut, S. d-f Heterobimetallic Association between Ytterbium and Ruthenium Carbon-Rich Complexes: Redox Commutation of Near-IR Luminescence. *Journal of the American Chemical Society* **2011,** 133, 6174-6176.
21. Norel, L.; Di Piazza, E.; Feng, M.; Vacher, A.; He, X. Y.; Roisnel, T.; Maury, O.; Rigaut, S. Lanthanide Sensitization with Ruthenium Carbon-Rich Complexes and Redox Commutation of Near-IR Luminescence. *Organometallics* **2014,** 33, 4824-4835.
22. Wong, K. M. C.; Lam, S. C. F.; Ko, C. C.; Zhu, N. Y.; Yam, V. W. W.; Roue, S.; Lapinte, C.; Fathallah, S.; Costuas, K.; Kahlal, S.; Halet, J. F. Electroswitchable photoluminescence activity: Synthesis, spectroscopy, electrochemistry, photophysics, and X-ray crystal and electronic structures of Re(bpy)(CO)(3)(C equivalent to C-C6H4-C equivalent to C)Fe(C5Me5)(dppe) PF6 (n) (n=0, 1). *Inorganic Chemistry* **2003,** 42, 7086-7097.

23. Liu, Y. F.; Ndiaye, C. M.; Lagrost, C.; Costuas, K.; Choua, S.; Turek, P.; Norel, L.; Rigaut, S. Diarylethene-Containing Carbon-Rich Ruthenium Organometallics: Tuning of Electrochromism. *Inorganic Chemistry* **2014,** 53, 8172-8188.
24. Anger, E.; Srebro, M.; Vanthuyne, N.; Toupet, L.; Rigaut, S.; Roussel, C.; Autschbach, J.; Crassous, J.; Reau, R. Ruthenium-Vinylhelicenes: Remote Metal-Based Enhancement and Redox Switching of the Chiroptical Properties of a Helicene Core. *Journal of the American Chemical Society* **2012,** 134, 15628-15631.
25. Li, B.; Wang, J.-Y.; Wen, H.-M.; Shi, L.-X.; Chen, Z.-N. Redox-Modulated Stepwise Photochromism in a Ruthenium Complex with Dual Dithienylethene-Acetylides. *Journal of the American Chemical Society* **2012,** 134, 16059-16067.
26. Mulas, A.; He, X.; Hervault, Y.-M.; Norel, L.; Rigaut, S.; Lagrost, C. Dual-Responsive Molecular Switches Based on Dithienylethene–RuII Organometallics in Self-Assembled Monolayers Operating at Low Voltage. *Chemistry – A European Journal* **2017,** 23, 10205-10214.
27. Ou, Y.-P.; Zhang, J.; Zhang, M.-X.; Zhang, F.; Kuang, D.; Hartl, F.; Liu, S. H. Bonding and Electronic Properties of Linear Diethynyl Oligothienoacene-Bridged Diruthenium Complexes and Their Oxidized Forms. *Inorg. Chem.* **2017,** 56, 11074-11086.
28. Burgun, A.; Gendron, F.; Sumby, C. J.; Roisnel, T.; Cador, O.; Costuas, K.; Halet, J.-F.; Bruce, M. I.; Lapinte, C. Hexatriynediyl Chain Spanning Two Cp*(dppe)M Termini (M = Fe, Ru): Evidence for the Dependence of Electronic and Magnetic Couplings on the Relative Orientation of the Termini. *Organometallics* **2014,** 33, 2613-2627.
29. Ying, J.-W.; Liu, I. P.-C.; Xi, B.; Song, Y.; Campana, C.; Zuo, J.-L.; Ren, T. Linear Trimer of Diruthenium Linked by Butadiyn-Diyl Units: A Unique Electronic Wire. *Angewandte Chemie-International Edition* **2010,** 49, 954-957.
30. Norel, L.; Bernot, K.; Feng, M.; Roisnel, T.; Caneschi, A.; Sessoli, R.; Rigaut, S. A carbon-rich ruthenium decorated dysprosium single molecule magnet. *Chemical Communications* **2012,** 48, 3948-3950.
31. Norel, L.; Feng, M.; Bernot, K.; Roisnel, T.; Guizouarn, T.; Costuas, K.; Rigaut, S. Redox Modulation of Magnetic Slow Relaxation in a 4f-Based Single-Molecule Magnet with a 4d Carbon-Rich Ligand. *Inorganic Chemistry* **2014,** 53, 2361-2363.
32. Liu, K.; Wang, X.; Wang, F. Probing Charge Transport of Ruthenium-Complex-Based Molecular Wires at the Single-Molecule Level. *Acs Nano* **2008,** 2, 2315-2323.
33. Rigaut, S. Metal complexes in molecular junctions. *Dalton Transactions* **2013,** 42, 15859-15863.
34. Mahapatro, A. K.; Ying, J.; Ren, T.; Janes, D. B. Electronic transport through ruthenium-based redox-active molecules in metal-molecule-metal nanogap junctions. *Nano Letters* **2008,** 8, 2131-2136.
35. Meng, F. B.; Hervault, Y. M.; Norel, L.; Costuas, K.; Van Dyck, C.; Geskin, V.; Cornil, J.; Hng, H. H.; Rigaut, S.; Chen, X. D. Photo-modulable molecular transport junctions based on organometallic molecular wires. *Chemical Science* **2012,** 3, 3113-3118.
36. Meng, F. B.; Hervault, Y. M.; Shao, Q.; Hu, B. H.; Norel, L.; Rigaut, S.; Chen, X. D. Orthogonally modulated molecular transport junctions for resettable electronic logic gates. *Nature Communications* **2014,** 5, 9.
37. Lissel, F.; Schwarz, F.; Blacque, O.; Riel, H.; Loertscher, E.; Venkatesan, K.; Berke, H. Organometallic Single-Molecule Electronics: Tuning Electron Transport through X(diphosphine)(2)FeC4Fe(diphosphine)(2)X Building Blocks by Varying the Fe-X-Au Anchoring Scheme from Coordinative to Covalent. *Journal of the American Chemical Society* **2014,** 136, 14560-14569.
38. Schwarz, F.; Kastlunger, G.; Lissel, F.; Riel, H.; Venkatesan, K.; Berke, H.; Stadler, R.; Loertscher, E. High-Conductive Organometallic Molecular Wires with De localized Electron Systems Strongly Coupled to Metal Electrodes. *Nano Letters* **2014,** 14, 5932-5940.
39. Marques-Gonzalez, S.; Yufit, D. S.; Howard, J. A. K.; Martin, S.; Osorio, H. M.; Garcia-Suarez, V. M.; Nichols, R. J.; Higgins, S. J.; Cea, P.; Low, P. J. Simplifying the conductance profiles of molecular junctions: the use of the trimethylsilylethynyl moiety as a molecule-gold contact. *Dalton Transactions* **2013,** 42, 338-341.

40. Quardokus, R. C.; Lu, Y.; Wasio, N. A.; Lent, C. S.; Justaud, F.; Lapinte, C.; Kandel, S. A. Through-Bond versus Through-Space Coupling in Mixed-Valence Molecules: Observation of Electron Localization at the Single-Molecule Scale. *Journal of the American Chemical Society* **2012,** 134, 1710-1714.
41. Wen, H.-M.; Yang, Y.; Zhou, X.-S.; Liu, J.-Y.; Zhang, D.-B.; Chen, Z.-B.; Wang, J.-Y.; Chen, Z.-N.; Tian, Z.-Q. Electrical conductance study on 1,3-butadiyne-linked dinuclear ruthenium(II) complexes within single molecule break junctions. *Chemical Science* **2013,** 4, 2471-2477.
42. Balesteros, L. M.; Martin, S.; Marques-Gonzalez, S.; Lopez, M. C.; Higgins, S. J.; Nichols, R. J.; Low, P. J.; Cea, P. Single Gold Atom Containing Oligo(phenylene)ethynylene: Assembly into LB Films and Electrical Characterization. *Journal of Physical Chemistry C* **2015,** 119, 784-793.
43. Schwarz, F.; Kastlunger, G.; Lissel, F.; Egler-Lucas, C.; Semenov, S. N.; Venkatesan, K.; Berke, H.; Stadler, R.; Lortscher, E. Field-induced conductance switching by charge-state alternation in organometallic single-molecule junctions. *Nature Nanotechnology* **2016,** 11, 170-176.
44. Al-Owaedi, O. A.; Milan, D. C.; Oerthel, M. C.; Bock, S.; Yufit, D. S.; Howard, J. A. K.; Higgins, S. J.; Nichols, R. J.; Lambert, C. J.; Bryce, M. R.; Low, P. J. Experimental and Computational Studies of the Single-Molecule Conductance of Ru(II) and Pt(II) trans-Bis(acetylide) Complexes. *Organometallics* **2016,** 35, 2944-2954.
45. Blum, A. S.; Ren, T.; Parish, D. A.; Trammell, S. A.; Moore, M. H.; Kushmerick, J. G.; Xu, G.-L.; Deschamps, J. R.; Pollack, S. K.; Shashidhar, R. Ru2(ap)4(σ-oligo(phenyleneethynyl)) Molecular Wires: Synthesis and Electronic Characterization. *J. Am. Chem. Soc.* **2005,** 127, 10010-10011.
46. Schull, T. L.; Kushmerick, J. G.; Patterson, C. H.; George, C.; Moore, M. H.; Pollack, S. K.; Shashidhar, R. Ligand Effects on Charge Transport in Platinum(II) Acetylides. *J. Am. Chem. Soc.* **2003,** 125, 3202-3203.
47. Olivier, C.; Costuas, K.; Choua, S.; Maurel, V.; Turek, P.; Saillard, J. Y.; Touchard, D.; Rigaut, S. "Chain-Like" Trimetallic Ruthenium Complexes with C-7 Carbon-Rich Bridges: Experimental and Theoretical Investigations of Electronic Communication Tuning in Five Distinct Oxidation States. *Journal of the American Chemical Society* **2010,** 132, 5638-5651.
48. Wuttke, E.; Pevny, F.; Hervault, Y.-M.; Norel, L.; Drescher, M.; Winter, R. F.; Rigaut, S. Fully Delocalized (Ethynyl)(vinyl)phenylene Bridged Triruthenium Complexes in up to Five Different Oxidation States. *Inorganic Chemistry* **2012,** 51, 1902-1915.
49. Olivier, C.; Choua, S.; Turek, P.; Touchard, D.; Rigaut, S. Electronic communication in "chain-like" trimetallic ruthenium complexes with two C-7 carbon-rich conjugated bridges. *Chemical Communications* **2007**, 3100-3102.
50. Field, L. D.; Magill, A. M.; Shearer, T. K.; Colbran, S. B.; Lee, S. T.; Dalgarno, S. J.; Bhadbhade, M. M. Controlled Synthesis of Dinuclear Acetylide-Bridged Ruthenium Complexes. *Organometallics* **2010,** 29, 957-965.
51. Wuttke, E.; Hervault, Y. M.; Polit, W.; Linseis, M.; Erler, P.; Rigaut, S.; Winter, R. F. Divinylphenylene- and Ethynylvinylphenylene-Bridged Mono-, Di-, and Triruthenium Complexes for Covalent Binding to Gold Electrodes. *Organometallics* **2014,** 33, 4672-4686.
52. Kahn, O. *Molecular Magnetism*. 1993.
53. *Magnetism: Molecules to Materials*. 2001.
54. Ratera, I.; Veciana, J. Playing with organic radicals as building blocks for functional molecular materials. *Chem. Soc. Rev.* **2012,** 41, 303-349.
55. Ohkoshi, S. I.; Tokoro, H. Photomagnetism in Cyano-Bridged Bimetal Assemblies. *Acc. Chem. Res.* **2012,** 45, 1749-1758.
56. Takamatsu, S.; Ishikawa, T.; Koshihara, S.-y.; Ishikawa, N. Significant increase of the barrier energy for magnetization reversal of a single-4f-ionic single-molecule magnet by a longitudinal contraction of the coordination space. *Inorganic Chemistry* **2007,** 46, 7250-7252.
57. Ishikawa, N.; Sugita, M.; Tanaka, N.; Ishikawa, T.; Koshihara, S. Y.; Kaizu, Y. Upward temperature shift of the intrinsic phase lag of the magnetization of bis(phthalocyaninato)terbium by ligand oxidation creating an S = (1)/(2) spin. *Inorganic Chemistry* **2004,** 43, 5498-5500.
58. Fortier, S.; Le Roy, J. J.; Chen, C.-H.; Vieru, V.; Murugesu, M.; Chibotaru, L. F.; Mindiola, D. J.; Caulton, K. G. A Dinuclear Cobalt Complex Featuring Unprecedented Anodic and Cathodic

Redox Switches for Single-Molecule Magnet Activity. *Journal of the American Chemical Society* **2013,** 135, 14670-14678.
59. Gonidec, M.; Davies, E. S.; McMaster, J.; Amabilino, D. B.; Veciana, J. Probing the Magnetic Properties of Three Interconvertible Redox States of a Single-Molecule Magnet with Magnetic Circular Dichroism Spectroscopy. *Journal of the American Chemical Society* **2010,** 132, 1756-+.
60. Gonidec, M.; Krivokapic, I.; Vidal-Gancedo, J.; Davies, E. S.; McMaster, J.; Gorun, S. M.; Veciana, J. Highly Reduced Double-Decker Single-Molecule Magnets Exhibiting Slow Magnetic Relaxation. *Inorganic Chemistry* **2013,** 52, 4464-4471.
61. Nava, A.; Rigamonti, L.; Zangrando, E.; Sessoli, R.; Wernsdorfer, W.; Cornia, A. Redox-Controlled Exchange Bias in a Supramolecular Chain of Fe-4 Single-Molecule Magnets. *Angewandte Chemie-International Edition* **2015,** 54, 8777-8782.
62. Freedman, D. E.; Jenkins, D. M.; Iavarone, A. T.; Long, J. R. A redox-switchable single-molecule magnet incorporating Re(CN)(7) (3-). *Journal of the American Chemical Society* **2008,** 130, 2884-2885.
63. Lanznaster, M.; Heeg, M. J.; Yee, G. T.; McGarvey, B. R.; Verani, C. N. Design of molecular scaffolds based on unusual geometries for magnetic modulation of spin-diverse complexes with selective redox response. *Inorganic Chemistry* **2007,** 46, 72-78.
64. Min, K. S.; Rheingold, A. L.; DiPasquale, A.; Miller, J. S. Characterization of the chloranilate(center dot 3-) pi radical as a strong spin-coupling bridging ligand. *Inorganic Chemistry* **2006,** 45, 6135-6137.
65. Ito, A.; Nakano, Y.; Urabe, M.; Kato, T.; Tanaka, K. Triradical cation of p-phenylenediamine having two nitroxide radical groups: Spin alignment mediated by delocalized spin. *Journal of the American Chemical Society* **2006,** 128, 2948-2953.
66. Lee, J.; Lee, E.; Kim, S.; Bang, G. S.; Shultz, D. A.; Schmidt, R. D.; Forbes, M. D. E.; Lee, H. Nitronyl Nitroxide Radicals as Organic Memory Elements with Both n- and p-Type Properties. *Angewandte Chemie-International Edition* **2011,** 50, 4414-4418.
67. Newton, G. N.; Yamashita, S.; Hasumi, K.; Matsuno, J.; Yoshida, N.; Nihei, M.; Shiga, T.; Nakano, M.; Nojiri, H.; Wernsdorfer, W.; Oshio, H. Redox-Controlled Magnetic {Mn-13} Keggin Systems. *Angewandte Chemie-International Edition* **2011,** 50, 5715-5719.
68. Matsumoto, I.; Ciofini, I.; Laine, P. P.; Teki, Y. Intramolecular Spin Alignment within Mono-Oxidized and Photoexcited Anthracene-Based pi Radicals as Prototypical Photomagnetic Molecular Devices: Relationships Between Electrochemical, Photophysical, and Photochemical Control Pathways. *Chemistry-a European Journal* **2009,** 15, 11210-11220.
69. Ferrando-Soria, J.; Castellano, M.; Ruiz-Garcia, R.; Cano, J.; Julve, M.; Lloret, F.; Pasan, J.; Ruiz-Perez, C.; Canadillas-Delgado, L.; Li, Y.; Journaux, Y.; Pardo, E. Redox switching of the antiferromagnetic coupling in permethylated dicopper(II) paracyclophanes. *Chemical Communications* **2012,** 48, 8401-8403.
70. Mukherjee, C.; Hoeke, V.; Stammler, A.; Boegge, H.; Schnack, J.; Glaser, T. Switching from antiferromagnetic to ferromagnetic coupling in heptanuclear (M6Mc)-M-t (n+) complexes by going from an achiral to a chiral triplesalen ligand. *Dalton Transactions* **2014,** 43, 9690-9703.
71. Schweinfurth, D.; Rechkemmer, Y.; Hohloch, S.; Deibel, N.; Peremykin, I.; Fiedler, J.; Marx, R.; Neugebauer, P.; van Slageren, J.; Sarkar, B. Redox-Induced Spin-State Switching and Mixed Valency in Quinonoid-Bridged Dicobalt Complexes. *Chemistry-a European Journal* **2014,** 20, 3475-3486.
72. Stroh, C.; Mayor, M.; von Hanisch, C.; Turek, P. Intramolecular exchange interaction in twofold spin-labelled platinum complexes. *Chemical Communications* **2004**, 2050-2051.
73. Di Piazza, E.; Merhi, A.; Norel, L.; Choua, S.; Turek, P.; Rigaut, S. Ruthenium Carbon-Rich Complexes as Redox Switchable Metal Coupling Units. *Inorganic chemistry* **2015,** 54, 6347-55.
74. Sakane, A.; Kumada, H.; Karasawa, S.; Koga, N.; Iwamura, H. Molecular structures and magnetic properties of the mixed-ligand complexes of bis(hexafluoroacetylacetonato)manganese(II), -copper(II), and -zinc(II) with 4,4'-bis(N-tert-butyl-N-oxylamino)-2,2'-bipyridine. Isosceles triangular hetero-three-spin systems consisting of aminoxyls and metal ions. *Inorganic Chemistry* **2000,** 39, 2891-2896.

75. Britten, J.; Hearns, N. G. R.; Preuss, K. E.; Richardson, J. F.; Bin-Salamon, S. Mn(II) and Cu(II) complexes of a dithiadiazolyl radical ligand: Monomer/dimer equilibria in solution. *Inorganic Chemistry* **2007,** 46, 3934-3945.
76. Koutsantonis, G. A.; Low, P. J.; Mackenzie, C. F. R.; Skelton, B. W.; Yufit, D. S. Coordinating Tectons: Bimetallic Complexes from Bipyridyl Terminated Group 8 Alkynyl Complexes. *Organometallics* **2014,** 33, 4911-4922.
77. Koutsantonis, G. A.; Jenkins, G. I.; Schauer, P. A.; Szczepaniak, B.; Skelton, B. W.; Tan, C.; White, A. H. Coordinating Tectons: Bipyridyl-Terminated Group 8 Alkynyl Complexes. *Organometallics* **2009,** 28, 2195-2205.
78. Packheiser, R.; Ecorchard, P.; Walfort, B.; Lang, H. Heterotrimetallic and heterotetrametallic transition metal complexes. *Journal of Organometallic Chemistry* **2008,** 693, 933-946.
79. Ota, A.; Ouahab, L.; Golhen, S.; Cador, O.; Yoshida, Y.; Saito, G. Paramagnetic transition metal complexes with a redox-active ligand: M(hfac)(2)(EDO-EDT-TTF-py)(n); M = Cu-II, n=1, 2; M = Mn-II, n=2. *New Journal of Chemistry* **2005,** 29, 1135-1140.
80. Norel, L.; Feng, M.; Bernot, K.; Roisnel, T.; Guizouarn, T.; Costuas, K.; Rigaut, S. Redox Modulation of Magnetic Slow Relaxation in a 4f-Based Single-Molecule Magnet with a 4d Carbon-Rich Ligand. *Inorg. Chem.* **2014,** 53, 2361-2363.
81. Alvarez, S.; Avnir, D.; Llunell, M.; Pinsky, M. Continuous symmetry maps and shape classification. The case of six-coordinated metal compounds (vol 26, pg 996, 2002). *New Journal of Chemistry* **2002,** 26.
82. Wuttke, E.; Pevny, F.; Hervault, Y. M.; Norel, L.; Drescher, M.; Winter, R. F.; Rigaut, S. Fully Delocalized (Ethynyl)(vinyl)phenylene Bridged Triruthenium Complexes in up to Five Different Oxidation States. *Inorganic Chemistry* **2012,** 51, 1902-1915.
83. Gauthier, N.; Tchouar, N.; Justaud, F.; Argouarch, G.; Cifuentes, M. P.; Toupet, L.; Touchard, D.; Halet, J. F.; Rigaut, S.; Humphrey, M. G.; Costuas, K.; Paul, F. Bonding and Electron Delocalization in Ruthenium(III) sigma-Arylacetylide Radicals trans-Cl(eta(2)-dppe)(2)RuC C(4-C6H4X) (+) (X = NO2, C(O)H, C(O)Me, F, H, OMe, NMe2): Misleading Aspects of the ESR Anisotropy. *Organometallics* **2009,** 28, 2253-2266.
84. Pevny, F.; Di Piazza, E.; Norel, L.; Drescher, M.; Winter, R. F.; Rigaut, S. Fully Delocalized (Ethynyl)(vinyl)phenylene-Bridged Diruthenium Radical Complexes. *Organometallics* **2010,** 29, 5912-5918.
85. Powell, C. E.; Cifuentes, M. P.; McDonagh, A. M.; Hurst, S. K.; Lucas, N. T.; Delfs, C. D.; Stranger, R.; Humphrey, M. G.; Houbrechts, S.; Asselberghs, I.; Persoons, A.; Hockless, D. C. R. Organometallic complexes for nonlinear optics. Part 27. Syntheses and optical properties of some iron, ruthenium and osmium alkynyl complexes. *Inorg. Chim. Acta* **2003,** 352, 9-18.
86. Horikoshi, R.; Nambu, C.; Mochida, T. Metal-centered ferrocene clusters from 5-ferrocenylpyrimidine and ferrocenylpyrazine. *Inorganic Chemistry* **2003,** 42, 6868-6875.
87. Senechal, K.; Toupet, L.; Ledoux, I.; Zyss, J.; Le Bozec, H.; Maury, O. First lanthanide dipolar complexes for second-order nonlinear optics. *Chemical Communications* **2004**, 2180-2181.
88. Marqués-González, S.; Parthey, M.; Yufit, D. S.; Howard, J. A. K.; Kaupp, M.; Low, P. J. Combined Spectroscopic and Quantum Chemical Study of [trans-Ru(C≡CC6H4R1-4)2(dppe)2]n+ and [trans-Ru(C≡CC6H4R1-4)(C≡CC6H4R2-4)(dppe)2]n+ (n = 0, 1) Complexes: Interpretations beyond the Lowest Energy Conformer Paradigm. *Organometallics* **2014,** 33, 4947-4963.
89. Kambe, K. On the paramagnetic susceptibilities of some polynuclear complex salts. *Journal of the Physical Society of Japan* **1950,** 5, 48-51.
90. Lloret, F.; Julve, M.; Cano, J.; Ruiz-Garcia, R.; Pardo, E. Magnetic properties of six-coordinated high-spin cobalt(II) complexes: Theoretical background and its application. *Inorganica Chimica Acta* **2008,** 361, 3432-3445.
91. Sharma, A. K.; Lloret, F.; Mukherjee, R. Phenolate- and Acetate (Both mu(2)-1,1 and mu(2)-1,3 Modes)-Bridged Linear Co-3(II) and (Co2MnII)-Mn-II Trimers: Magnetostructural Studies. *Inorganic Chemistry* **2013,** 52, 4825-4833.
92. Zhao, Q. H.; Li, H. F.; Chen, Z. D.; Fang, R. B. Synthesis, crystal structures and magnetic properties of Co-3(NCS)(6)(admtrz)(6) center dot CH3OH center dot H2O and Ni-

3(NCS)(6)(admtrz)(6) center dot 1.5H(2)O (admtrz=4-amino-3,5-dimethyl-1,2,4-triazole). *Inorganica Chimica Acta* **2002,** 336, 142-146.
93. Van Albada, G. A.; de Graaff, R. A. G.; Haasnoot, J. G.; Reedijk, J. Synthesis, spectroscopic characterization, and magnetic-properties of unusual 3,5-dialkyl-1,2,4-triazole compounds containing N-bridging isothiocyanato ligands - x-ray structure of trinuclear bis (mu-thiocyanato-N)bis(mu-3,5-diethyl-1,2,4-triazole-N1,N2)bis(thiocyanato-N)(3,5-diethyl-1,2,4-triazole-n1)nickel(II)-N,N1,N1' nickel(II) dihydratect. *Inorganic Chemistry* **1984,** 23, 1404-1408.
94. Ginsberg, A. P.; Martin, R. L.; Sherwood, R. C. Magnetic exchange in transition metal complexes .4. Linear trimeric bis(acetylacetonato)nickel(2). *Inorganic Chemistry* **1968,** 7, 932-936.
95. Mackey, D. J.; Martin, R. L. Low-temperature magnetic studies of a linear trimeric nickel compound - abcjkl-hexa-aqua-def-ghi-hexakis mu-1,2,4-triazole-n1n2)-trinickel(ii)he xanitrate dihydrate. *J. Chem. Soc., Dalton Trans.* **1978**, 702-704.
96. Guo, J. F.; Wang, X. T.; Wang, B. W.; Xu, G. C.; Gao, S.; Szeto, L.; Wong, W. T.; Wong, W. Y.; Lau, T. C. One-Dimensional Ferromagnetically Coupled Bimetallic Chains Constructed with trans- Ru(acac)(2)(CN)(2) (-): Syntheses, Structures, Magnetic Properties, and Density Functional Theoretical Study. *Chemistry-a European Journal* **2010,** 16, 3524-3535.
97. Noodleman, l. Valence bond description of anti-ferromagnetic coupling in transition-metal dimers. *J. Chem. Phys.* **1981,** 74, 5737-5743.
98. Broer, R.; de Graaf, C. *Magnetic Interactions in Molecules and Solids*. Springer International Publishing: 2015.
99. Maneru, D. R.; Costa, R.; Marquez, M. G.; Moreira, I. D. R.; Illas, F. Handling Magnetic Coupling in Trinuclear Cu(II) Complexes. *Journal of Chemical Theory and Computation* **2015,** 11, 3650-3660.
100. Caballol, R.; Castell, O.; Illas, F.; Moreira, P. R.; Malrieu, J. P. Remarks on the proper use of the broken symmetry approach to magnetic coupling. *J. Phys. Chem. A* **1997,** 101, 7860-7866.
101. Valero, R.; Costa, R.; Moreira, I.; Truhlar, D. G.; Illas, F. Performance of the M06 family of exchange-correlation functionals for predicting magnetic coupling in organic and inorganic molecules. *J. Chem. Phys.* **2008,** 128.
102. Rivero, P.; Moreira, I. D. R.; Illas, F.; Scuseria, G. E. Reliability of range-separated hybrid functionals for describing magnetic coupling in molecular systems. *Journal of Chemical Physics* **2008,** 129.
103. Allen, H. C.; Kokoszka, G. F.; Inskeep, R. G. The Electron Paramagnetic Resonance Spectrum of Some Tris-Complexes of Copper(II). *J. Am. Chem. Soc.* **1964,** 86, 1023-1025.
104. Castillo, O.; Luque, A.; Román, P. Synthesis, chemical characterization and crystal structure of the (oxalato-O,O′)bis(1,10-phenanthroline)copper(II) pentahydrate. *J. Mol. Struct.* **2001,** 570, 181-188.
105. Rigaut, S.; Olivier, C.; Costuas, K.; Choua, S.; Fadhel, O.; Massue, J.; Turek, P.; Saillard, J. Y.; Dixneuf, P. H.; Touchard, D. C-7 and C-9 carbon-rich bridges in diruthenium systems: Synthesis, spectroscopic, and theoretical investigations of different oxidation states. *Journal of the American Chemical Society* **2006,** 128, 5859-5876.
106. Stoll, S.; Schweiger, A. EasySpin, a comprehensive software package for spectral simulation and analysis in EPR. *J. Magn. Res.* **2006,** 178, 42-55.
107. Altomare, A.; Burla, M. C.; Camalli, M.; Cascarano, G. L.; Giacovazzo, C.; Guagliardi, A.; Moliterni, A. G. G.; Polidori, G.; Spagna, R. SIR97: a new tool for crystal structure determination and refinement. *Journal of Applied Crystallography* **1999,** 32, 115-119.
108. Sheldrick, G. M. A short history of SHELX. *Acta Crystallographica Section A* **2008,** 64, 112-122.
109. Farrugia, L. WinGX suite for small-molecule single-crystal crystallography. *Journal of Applied Crystallography* **1999,** 32, 837-838.
110. van der Sluis, P.; Spek, A. L. Bypass - an effective method for the refinement of crystal-structures containing disordered solvent regions. *Acta Crystallographica Section A* **1990,** 46, 194-201.
111. Spek, A. PLATON, An Integrated Tool for the Analysis of the Results of a Single Crystal Structure Determination. *Acta Crystallographica Section A* **1990,** 46, c34.

112. Fonseca Guerra, C. F.; Snijders, J. G.; te Velde, G.; Baerends, E. J. Towards an order-N DFT method. *Theor. Chem. Acc.* **1998,** 99, 391-403.
113. te Velde, G.; Bickelhaupt, F. M.; Baerends, E. J.; Fonseca Guerra, C.; van Gisbergen, S. J. A.; Snijders, J. G.; Ziegler, T. Chemistry with ADF. *J. Comput. Chem.* **2001,** 22, 931-967.
114. *Amsterdam Density Functional (ADF)*, 2016.01; SCM, Theoretical Chemistry, Vrije Universiteit: Amsterdam, The Netherlands, 2016.
115. Vosko, S. H.; Wilk, L.; Nusair, M. Accurate spin-dependent electron liquid correlation energies for local spin-density calculations - a critical analysis. *Canadian Journal of Physics* **1980,** 58, 1200-1211.
116. Becke, A. D. Density-functional thermochemistry .3. The role of exact exchange. *Journal of Chemical Physics* **1993,** 98, 5648-5652.
117. Perdew, J. P. Density-functional approximation for the correlation-energy of the inhomogeneous electron-gas. *Physical Review B* **1986,** 33, 8822-8824.
118. Versluis, L.; Ziegler, T. The determination of molecular-structures by density functional theory - the evaluation of analytical energy gradients by numerical-integration. *Journal of Chemical Physics* **1988,** 88, 322-328.
119. Zahlan, A.; Heineken, F. W.; Bruin, M.; Bruin, F. ESR Spectrum of 2,2′ Dipyridyl-Na Complex. *J. Chem. Phys.* **1962,** 37, 683-684.
120. Stephens, P. J.; Devlin, F. J.; Chabalowski, C. F.; Frisch, M. J. Ab-initio calculation of vibrational absorption and circular-dichroism spectra using density-functional force-fields. *Journal of Physical Chemistry* **1994,** 98, 11623-11627.
121. Adamo, C.; Barone, V. Toward reliable density functional methods without adjustable parameters: The PBE0 model. *Journal of Chemical Physics* **1999,** 110, 6158-6170.
122. Ernzerhof, M.; Scuseria, G. E. Assessment of the Perdew-Burke-Ernzerhof exchange-correlation functional. *Journal of Chemical Physics* **1999,** 110, 5029-5036.
123. Zhao, Y.; Truhlar, D. G. A new local density functional for main-group thermochemistry, transition metal bonding, thermochemical kinetics, and noncovalent interactions. *Journal of Chemical Physics* **2006,** 125.
124. Zhao, Y.; Truhlar, D. G. The M06 suite of density functionals for main group thermochemistry, thermochemical kinetics, noncovalent interactions, excited states, and transition elements: two new functionals and systematic testing of four M06-class functionals and 12 other functionals. *Theoretical Chemistry Accounts* **2008,** 120, 215-241.
125. *ADF-GUI*, 2014; SCM, Theoretical Chemistry, Vrije Universiteit: Amsterdam, The Netherlands.